AD_____

GRANT NUMBER DAMD17-94-J-4314

TITLE: Molecular Analysis of Motility in Metastatic Mammary Adenocarcinoma Cells

PRINCIPAL INVESTIGATOR: Jeffrey E. Segall, Ph.D.

CONTRACTING ORGANIZATION: Albert Einstein College of Medicine
of Yeshiva University
Bronx, New York 10461

REPORT DATE: September 1998

TYPE OF REPORT: Final

PREPARED FOR: Commander
U.S. Army Medical Research and Materiel Command
Fort Detrick, Frederick, Maryland 21702-5012

REPORT DOCUMENTATION PAGE

Form Approved
OMB No. 0704-0188

1. AGENCY USE ONLY *(Leave blank)*	2. REPORT DATE	3. REPORT TYPE AND DATES COVERED
	September 1998	Final (26 Aug 94 - 25 Aug 98)

4. TITLE AND SUBTITLE
Molecular Analysis of Motility in Metastatic Mammary Adenocarcinoma Cells

5. FUNDING NUMBERS
DAMD17-94-J-4314

6. AUTHOR(S)
Jeffrey E. Segall, Ph.D.

7. PERFORMING ORGANIZATION NAME(S) AND ADDRESS(ES)
Albert Einstein College of Medicine
of Yeshiva University
Bronx, New York 10461

8. PERFORMING ORGANIZATION REPORT NUMBER

9. SPONSORING/MONITORING AGENCY NAME(S) AND ADDRESS(ES)
Commander
U.S. Army Medical Research and Materiel Command
Fort Detrick, Frederick, Maryland 21702-5012

10. SPONSORING/MONITORING AGENCY REPORT NUMBER

11. SUPPLEMENTARY NOTES

12a. DISTRIBUTION / AVAILABILITY STATEMENT
Approved for public release; distribution unlimited

12b. DISTRIBUTION CODE

13. ABSTRACT *(Maximum 200*

This final report provides (1) a detailed account of our analysis of the role of the Arp2/3 complex in mediating EGF-stimulated lamellipod extension, (2) a description of our results in producing cell lines expressing talin anti-sense RNA, and (3) a general summary of our understanding of the process of lamellipod extension in mammary adenocarcinoma cells, based upon the work supported by this grant. We find that the Arp 2/3 complex is present in parallel with filamentous actin at the leading edge. This localization is much broader that the distribution of EGF-stimulated nucleation sites and is more consistent with the Arp 2/3 complex functioning as a pointed end capper. We have produced cells expressing talin antisens mRNA which show a regulated 50% decrease in the amount of talin protein. The cells show reduced focal contacts and altered stress fiber distributions. However, EGF-stimulated lamellipod extension is not quantitatively altered. Talin localization to the leading edge appears to be tighter than localization to focal contacts. In summary, our results show that EGF stimulation of tumor cells produces a highly localized increase in actin nucleation (within 100 nm of the membrane) that is independent of interaction with the substratum.

14. SUBJECT TERMS
Breast Cancer ,cell motility, talin, Arp 2/3, EGF, chemotaxis

15. NUMBER OF PAGES
75

16. PRICE CODE

17. SECURITY CLASSIFICATION OF REPORT	18. SECURITY CLASSIFICATION OF THIS PAGE	19. SECURITY CLASSIFICATION OF ABSTRACT	20. LIMITATION OF ABSTRACT
Unclassified	Unclassified	Unclassified	Unlimited

FOREWORD

Opinions, interpretations, conclusions and recommendations are those of the author and are not necessarily endorsed by the U.S. Army.

____ Where copyrighted material is quoted, permission has been obtained to use such material.

____ Where material from documents designated for limited distribution is quoted, permission has been obtained to use the material.

____ Citations of commercial organizations and trade names in this report do not constitute an official Department of Army endorsement or approval of the products or services of these organizations.

JCT ____ In conducting research using animals, the investigator(s) adhered to the "Guide for the Care and Use of Laboratory Animals," prepared by the Committee on Care and use of Laboratory Animals of the Institute of Laboratory Resources, national Research Council (NIH Publication No. 86-23, Revised 1985).

____ For the protection of human subjects, the investigator(s) adhered to policies of applicable Federal Law 45 CFR 46.

JCT ____ In conducting research utilizing recombinant DNA technology, the investigator(s) adhered to current guidelines promulgated by the National Institutes of Health.

JCT ____ In the conduct of research utilizing recombinant DNA, the investigator(s) adhered to the NIH Guidelines for Research Involving Recombinant DNA Molecules.

JCT ____ In the conduct of research involving hazardous organisms, the investigator(s) adhered to the CDC-NIH Guide for Biosafety in Microbiological and Biomedical Laboratories.

Jeff C. Cegall 11/30/98

PI / Signature Date

TABLE OF CONTENTS

INTRODUCTION

Metastasis, Motility and EGF

Tumor spread beyond the primary sites remains the major life-threatening aspect of cancer, and thus more efforts are warranted to unveil major specific characteristics of metastatic tumor cells so that one could modify, or at least predict, the clinical course of the disease. Metastasis is a complex process involving a number of different biological phenomena that can amplify a tumor cell's ability to metastasize(1-9). Reduction in cell-cell contact, increased angiogenesis around the primary tumor, and evasion of immune system cells can play critical roles in enabling metastasis to proceed. During metastasis, malignant cells from the primary tumor invade the surrounding tissues, penetrate neighboring lymphatic or blood vessels, and disseminate via the circulation to distant organs where they can generate secondary tumors. The intravasation and extravasation processes are thought to include three essential steps: release of proteolytic enzymes which will degrade the surrounding extracellular matrix or basement membrane, active lamellipod extension through the newly created pathway towards the vessel wall, and formation of new attachments (with detachment from previous adhesion sites). The result of repeating these steps is the production of intrinsic cellular **motility** which enables the cell to actively make its way through surrounding tissue as well as into and out of blood vessels.

The EGF receptor (referred to also as ErbB1), as well as another member of the EGF receptor family, ErbB2 (also referred to as HER2 or neu), have been shown to correlate with poor prognosis in a number of tumor types, including small cell lung cancer, breast cancer, gastric cancer, and prostate cancer (10-16). Overexpression of ErbB1 or ErbB2 has been found to correlate with poor prognosis among breast cancer patients (13,15,17), and some studies have shown a significant negative correlation between expression of ErbB1 or ErbB2 and relapse free survival (18,19). Furthermore, it has been demonstrated that ErbB1 can be overexpressed in breast tumor metastases when compared to the primary tumor (20,21), which suggests a direct involvement of the expression of the EGF receptor in the metastatic process.

Treatment approaches involving targeting of tumor cells overexpressing either ErbB1 or ErbB2 are being developed (22-25).

The work described in this final report has focused on the mechanisms by which EGF stimulates motility and chemotaxis in the metastatic mammary adenocarcinoma cell line MTLn3. MTLn3 cells have high metastatic potential (26), are chemotactic to EGF (27) and express the cell surface receptor for EGF at normal levels (28) (29). In addition, the motile and chemotactic responses of MTLn3 cells have similarities to those seen in well-characterized cells such as *Dictyostelium* and neutrophils (27). Thus MTLn3 cells provide a powerful model system for the study of EGF involvement in cell motility, metastasis and tumor cell chemotaxis.

A key step in the process of cell movement is the generation of an actin filled leading edge, or lamellipod. Studies with highly motile cells such as *Dictyostelium* (30), neutrophils (31) and platelets (32) in particular have shown that stimulation of cells with chemoattractant generates a transient increase in actin polymerization activity in the actin cytoskeleton. It is unclear how stimulation of cell surface receptors is linked to actin polymerization. Actin polymerization could be stimulated by severing or uncapping of pre-existing actin filaments, increasing availability of polymerization competent monomeric actin, or by de novo assembly of new filaments (30) (31).

Achievement of Technical Objectives

Given the importance of chemoattractant-stimulated actin polymerization in cell motility and metastasis, the work funded by this grant was aimed at evaluating EGF-stimulated motility of metastatic breast cancer cells. The first technical objective was:
TECHNICAL OBJECTIVE 1. Determine the time course and dose response range of changes in cell motility and morphology after stimulation with EGF using time lapse microscopy. This determines the appropriate time scale and stimulus concentrations for performing the experiments described in TECHNICAL OBJECTIVE's 2 -3.

Task 1. Determine characteristics of behavioral responses of MTLn3 cells to EGF, Months 1 - 12:

a. Measure time course and dose response range of changes in area of MTLn3 cells in response to epidermal growth factor (EGF).
b. Compare chemotactic and chemokinetic responsiveness to EGF using a modified Boyden chamber.
c. Determine detailed responses of individual cells to a gradient of EGF produced by a micropipet.

This objective was accomplished and the results published in (27) and (33).

The second technical objective and accompanying task in the Statement of Work was:

TECHNICAL OBJECTIVE 2: Determine the role of actin capping proteins by: a) Studying the kinetics of actin nucleation and capping activity following stimulation of cells, and b) measuring the kinetics of aginactin and gelsolin association with the cytoskeleton.

Task 2. Evaluate the role of actin capping proteins in area changes induced by EGF, Months 12 - 18:

a. Determine if actin nucleation activity after stimulation with EGF.
b. If actin nucleation activity is activated, measure the kinetics of capping activity; a reciprocal relationship suggests the involvement of a capping protein.
c. Test whether either of the capping proteins, aginactin or gelsolin is responsible for the changes in capping activity by measuring the kinetics of association with cell actin filaments.
d. Use immunofluorescence to compare the location of the capping protein identified in 2c. with the location of F-actin in cells stimulated with EGF.

Task 2a was accomplished and the results published (34). An EGF-stimulated increase in actin nucleation was clearly demonstrated at the sites of lamellipod extension. However, further work by us and others then demonstrated that control of capping protein was unlikely to be the key step in chemoattractant-stimulated actin polymerization(34) (35,36). Either severing or de novo nucleation are currently the most likely mechanisms by which chemoattractants stimulate actin polymerization. Thus, the focus of this technical objective was altered to evaluate the relative roles of severing and nucleating factors.

The role of surface interactions was evaluated in more detail, because EGF-stimulated lamellipods are typically oriented parallel to the substratum and ruffling is suppressed(37). As published in (33), we determined that the initial adhesion status of the cells was critical in determining the shape of the protrusion induced by EGF, but that continuous connection with the substratum during protrusion extension was not required. This suggested that molecules that form the interface between integrins and the cytoskeleton might be important. Talin is a molecule that both binds to integrins and has been suggested as a potential nucleator of actin filaments (38) at the cell membrane. We evaluated the localization of talin at the light microscope level as a function of EGF stimulation and found that it localized at the leading edge of the cell, thus suggesting that it might be critical in the process of nucleated actin polymerization. Another potentially important nucleating factor is the Arp2/3 complex. To more precisely determine the likelihood of the Arp2/3 complex in nucleating actin polymerization in MTLn3 cells, we performed a high resolution EM study of the location of Arp2/3 relative to EGF-stimulated actin nucleation sites. This work is reported in the body of this report and has been submitted for publication.

Technical Objective 3 and the corresponding task from the Statement of Work were:
TECHNICAL OBJECTIVE 3: Measure actin crosslinking activity and compare with the association of ABP-280, EF-1alpha, and alpha-actinin with the cytoskeleton.

Task 3. Evaluate the role of actin crosslinking proteins in area changes induced by EGF, Months 18 - 24:

a. Measure the incorporation of actin into Triton-insoluble cytoskeletons as a function of time after stimulation with EGF.
b. Determine if any of the actin crosslinking proteins ABP280, EF-1alpha, and alpha-actinin are incorporated into the cytoskeleton with the time course measured in 3a.
c. Use immunofluorescence to determine if the actin crosslinking proteins identified in 3b are present in cell extensions induced by EGF.

Task 3a was accomplished as well as the parts of 3b and 3c relevant to EF1alpha and published in (39). The results of that study indicated that crosslinking per se occurred after the initial stimulation of actin polymerization, and therefore crosslinking proteins such as ABP280 and alpha-actinin were unlikely to be involved in the initial generation of nucleation sites.

Technical Objective 4 and its accompanying task in the Statement of Work was:
TECHNICAL OBJECTIVE 4: Based on the results in T. O.'s 1 -3, rank the proteins tested in terms of potential importance in mediating changes in cell motility or morphology after stimulation, and identify or acquire clones for the rat gene for the most important protein.

Task 4. Rank the proteins tested in Tasks 2 and 3, and acquire cDNA clones for the top ranking clones, Months 24 - 30.

a. The proteins tested n Tasks 2 and 3 will be ranked in terms of their potential importance in mediating changes in cell area induced by EGF; top ranking is assigned to proteins whose association with the cytoskeleton and localization in cell extensions correlates with the temporal changes in crosslinking or capping activity measured in cell lysates.

b. Acquire the rat cDNA clones for the top ranking clones; depending on information available this may involve collaborating if the cDNA has already been isolated or using PCR-based methods or library screening to isolate the clone.

From the studies performed in Technical Objectives 1 -3 as discussed above, we concluded that talin and the Arp 2/3 complex were potential mediators of the EGF-stimulated actin polymerization process in MTLn3 cells. At the time, talin clones were available and therefore we proceeded first with generating MTLn3 derived cell lines expressing an antisense talin promoter.

Technical Objective 5 and its accompanying task in the Statement of Work was:

TECHNICAL OBJECTIVE 5: Using clones for the protein chosen in TECHNICAL OBJECTIVE 4, alter expression of the protein and determine the effects on motility and metastatic capability.

Task 5. Alter the expression of the proteins identified in Task 4 and determine the effects on motility and metastasis, Months 30 - 48.

a. Using the cDNA sequence, select antisense oligonucleotides to reduce expression of the proteins in cells grown in culture; determine if a reduction in protein expression leads to an alteration in changes in area induced by EGF.
b. Insert the cDNA into transformation vectors in the antisense orientation.
c. Generate cell lines of stable transformants and compare protein expression, EGF-stimulated area changes, and metastatic capability of cell lines transformed with the antisense construct with cell lines transformed with a control vector (for analysis of metastasis, each cell line will be injected into at least 10 rats).

For our final technical objective, we have focussed on altering the expression of talin in MTLn3 cells in order to evaluate its role in lamellipod extension and metastasis. The current status of the work regarding MTLn3 cells expressing antisense talin mRNA will be described in the body of this report. For evaluation of other proteins that might be directly involved in control of actin polymerization during lamellipod extension, we have developed an electron microscope approach that provides much better spatial localization of proteins relative to sites of actin polymerization. This is important because colocalization at the light microscope level does not provide a clear separation between proteins that simply bind to actin filaments and proteins directly associated with the sites of actin polymerization.

MATERIALS AND METHODS

Cells

MTLn3 metastatic rat mammary adenocarcinoma cells were kindly provided by Dr. Garth Nicholson, MD Anderson Cancer Center, Houston, Texas. Cells were grown in alpha-MEM (Gibco), supplemented with 5% fetal calf serum and antibiotics as previously described (27). For all experiments, unless otherwise mentioned, MTLn3 cells were prepared as follows: cells were plated at low density in complete medium for about 24 hours, and starved for 3 hours prior to the experiment in alpha-MEM medium supplemented with 0.35% BSA and 12 mM Hepes (starvation medium). Stimulation was done with a final concentration of 5 nM murine EGF (Life Technologies) in starvation medium.

MTLn3 cells expressing talin antisense clones were generated as follows. The 5' end of the cDNA sequence for talin (76) was cloned in the antisense direction into pBPSTR-1. This vector is contains a tetracycline-regulated promoter such that the presence of tetracycline in the medium (or animal) suppresses expression of the antisense RNA. MTLn3 cells were transfected with the antisense construct and selected using hygromycin resistance. Stable clones were isolated and clones with reduced talin expression in the absence of tetracycline (compared to in the presence of tetracycline) were analyzed further.

Antibodies

Monospecific anti-Arp3, anti-p21 and anti-p34 rabbit polyclonal antibodies were kindly provided by Dr. Matthew Welch (Department of Cellular and Molecular Pharmacology, University of California, San Francisco), and have been previously characterized (40). Anti-actin monoclonal antibody was purchased from Boehringer Manheim. Cy5-conjugated goat anti-mouse IgG was purchased from Accurate Laboratories and Scientific Corporation. Fluorescein-conjugated goat anti-rabbit IgG was purchased from Cappel Laboratories. Goat anti-biotin antibodies coupled to

5 nm gold particles, and goat anti-rabbit antibodies coupled to 10 nm gold particles were purchased from Nanoprobes.

Light microscopy

Immunofluorescence. Cells were plated on coverslips on MatTek dishes (MatTek Corporation, Ashland, MA) or coverslips as previously described (33), and stimulated with EGF or left untreated. They were fixed for 5 min at 37°C with 3.7% formaldehyde in a buffer containing 5 mM KCl, 137 mM NaCl, 4 mM $NaHCO_3$, 0.4 mM KH_2PO_4, 1.1 mM Na_2HPO_4, 2 mM $MgCl_2$, 5 mM PIPES, 2 mM EGTA and 5.5 mM glucose (cytoskeleton stabilization buffer pH 6.1, (41). They were then treated with cold methanol for 2 min, rinsed and permeabilized for 20 minutes at room temperature in 0.5% Triton X100 in stabilization buffer. The cells were then rinsed once with 0.1 M glycine in stabilization buffer and incubated for a further 10 minutes in glycine. After 5 washes with TBS (Tris 20 mM, NaCl 154 mM, pH 8), the preparations were blocked/stabilized by incubation for 20 minutes with 5 uM phalloidin (Calbiochem) in TBS pH 8 supplemented with 1% BSA and 1 % fetal calf serum. Cells were further incubated for 1 hour with the primary antibodies followed by 5 rinses in TBS plus 1% BSA and incubation for 1 hour with Cy5-conjugated anti mouse antibodies and FITC-conjugated anti rabbit antibodies. After final washes, the coverslips were mounted in 50% glycerol in TBS supplemented with 6 mg/ml N-propyl gallate.

Nucleation site visualization and Arp2/3 colocalization. Nucleation sites were visualized using a previously described protocol (34) with slight modifications. Briefly, cells grown on MatTek dishes were stimulated with EGF, and permeabilized in presence of 0.45 uM Rhodamine-labeled actin (34) in Buffer C (138 mM KCl, 10 mM PIPES pH 6.9, 0.1 mM ATP, 3 mM EGTA pH 6.9, 4 mM MgCl2) + 1% BSA for 1 min. After a brief rinse in Buffer C, the cells were fixed in 3.7% formaldehyde in cytoskeleton stabilization buffer (see above) for 5 min, followed by a 10 min

incubation in 0.1 M glycine in cytoskeleton stabilization buffer. After a rinse in TBS, the samples were incubated with 5 uM phalloidin for 20' in TBS/BSA/FCS (pH 8.1, see above), washed 5 times for 5 min with TBS/BSA and mounted in glycerol 50% in TBS pH 8.1 + 6 mg/ml N-propyl gallate. For colocalization of nucleation sites and Arp3 or p21, the cells were permeabilized in presence of rhodamine-labeled actin and fixed with formaldehyde as above. The samples were further treated with methanol for 2 min before being processed for immunolabeling as described in the immunofluorescence protocol above, with the exception that the triton permeabilization step was omitted.

Fluorescence quantification. Images were taken using constant settings on an Olympus IX70 microscope with 60X, N.A.1.4 infinity corrected optics coupled to a computer driven cooled CCD camera using IPLab Spectrum software (Vaytek, Fairfield, IA). The digitized images were then converted linearly in NIH Image (program developed at the U.S. National Institutes of Health and available on the Internet at http://rsb.info.nih.gov/nih-image/), and analyzed using different macros. For measurement of the fluorescence from the leading edge back to ~3 um inside the cell, the macro gives the mean of pixel intensity within 1 pixel concentric perimeters, running from the outside of the cell to the inside (34). For the kinetic experiment, the mean fluorescence was evaluated within a 1.2 um band covering the whole cell perimeter at the leading edge.

Electron microscopy

Preparation of biotin-labeled actin. The biotin labeled actin was prepared according to Okabe and Hirokawa (42) with modifications. 25 mg of G-actin (alpha/rabbit skeletal muscle) was dialyzed for 24 hours in depolymerization buffer (2 mM Tris HCl, pH 7.5; 0.1 mM $CaCl_2$; 0.2 mM ATP). It was then clarified for 20 min at 95000 rpm in TL100 centrifuge, diluted to 3 mg/ml in depolymerization buffer above, and polymerized at room temperature for 2 hours by adding final concentrations of: 10 mM Tris HCl, pH 7.5; 2 mM $MgCl_2$; 100 mM KCl and 1 mM ATP.

Eight mg of NSH-biotin (Pierce) was then added to the solution, and biotinylation was allowed to proceed for 10 min at room temperature. The reaction was quenched by adding 100 mg of sodium glutamate, and the F-actin was pelleted. The actin was then run through two cycles of polymerization/depolymerization, where the G-actin suspension was polymerized by adding 2 mM $MgCl_2$, 50 mM KCl, 10 mM PIPES pH 7 in a water bath at RT for 1 hour, and depolymerized in buffer A (2 mM Tris pH 8, 0.2 mM $CaCl_2$, 0.02% NaN3, 0.2 mM ATP, 0.5 mM DTT). The actin was then purified on a gel filtration G150 column in buffer A. Storage was done in liquid nitrogen in 1 M sucrose. Initial coupling ratio was approximately 2 moles of biotin per mole of actin, but some loss occurred on storage. The biotin-labeled actin was found to have a polymerization activity comparable to that of unlabeled actin, both in terms of percent polymerizable at equilibrium (>90%) and polymerization rates (as measured by viscometry).

Preparation of biotin-labeled gelsolin-actin complex. Biotin-labeled gelsolin-actin complex (b-GA2) was prepared as described previously (34), using G-actin labeled with biotin as described above. For immunoelectron microscopy and colocalization with the Arp2/3 complex, 100 nM of the complex was used in place of biotin-actin in the permeabilization buffer and the preparations were further processed as described below.

Preparation of samples for negative staining. MTLn3 cells were grown on Formvar or Parlodion-carbon-coated gold square support grids (Electron Microscopy Science, Fort Washington, PA) on coverslips for 18-24 hours. The immunoelectron microscopy was based on a previously described protocol (43,44) with some modifications. The coverslips were treated with 0.25% Triton X-100 in Buffer C in presence of 1% BSA and 0.45 uM biotin labeled actin for 1 min. After a rapid wash in buffer C, the preparations were fixed with 0.5 % glutaraldehyde in cytoskeleton stabilization buffer pH 6-6.1 in the presence of 5 uM phalloidin for 10 min. The grids were then rinsed in cytoskeletal buffer and incubated for 15 min in 50 mM NH_4Cl in PBS (145.5 mM NaCl, 4 mM NaH_2PO_4, 6 mM $Na_2HPO_4.7H_2O$), with a change to fresh solution

after 7 min. This was followed by a 30 min incubation in 0.1% gelatin (IGSS gelatin, Amersham) in PBS, with a change to fresh solution after 15 min. The grids were then incubated for 6 hours with 5 nm gold-conjugated anti-biotin antibodies. They were then washed for 10 min 3 times in 0.1% gelatin, followed by 1 min in 0.05% Triton in PBS and four 1 min-washes in PBS. They were then post-fixed in 1% glutaraldehyde/5 uM phalloidin in cytoskeleton stabilization buffer for 15 min, and transferred briefly in cytoskeleton stabilization buffer before being negatively stained. For double labeling for actin and Arp2/3 complex, the grids were additionally methanol treated for 2 min before the NH_4Cl step, blocked for 30 min with gelatin, and incubated for 1.5-2 hours with anti-Arp3 or anti-p21 antibodies. The grids were then rinsed 3 times for 10 min in 0.1% gelatin, and incubated for 6 hours in a mixture of 5 nm-gold conjugated anti-biotin antibodies and 10 nm gold-conjugated anti rabbit antibodies. They were then washed and post-fixed as described above. For negative staining, the grids were sequentially transferred through 4 drops of 40 ug/ml of bacitracin in water, followed by 4 drops of 1% phosphotungstic acid. The grids were then blotted dry and observed using a JEOL 100CX transmission electron microscope at 80 kV.

Preparation of samples for rapid freezing, freeze drying and rotary shadowing (FDS). MTLn3 cells were grown on 5 mm glass coverslips and processed for immunoelectron microscopy as described above. After the post fixation step, the coverslips were rinsed 3 times in water and processed for FDS based on the procedure described by Hartwig (45). Briefly, the fixed coverslips were washed with 2 changes of distilled water. They were then placed on the specimen mount of the rapid freezing apparatus (Life Cell Corporation CF100), and frozen by slamming them into a liquid nitrogen-cooled cooper block. Freezing tabs containing the frozen coverslips were transferred to a liquid nitrogen-cooled stage of a Cressington CFE-50 freeze fracture apparatus, the stage temperature raised to -90°C for 90 min, and then rotary shadowed at a 45° angle with 1.2-1.3 nm tantalum-tungsten, followed by 2.5 nm carbon at 90°. Replicas were separated from the coverslip with 25% hydrofluoric acid, washed into distilled water, and picked

up on the surface of Formvar-coated copper grids. The samples were observed using a JEOL 100CX transmission electron microscope at 100 kV. Images were viewed as negatives for better contrast, the gold particles appearing white.

Morphometric analysis. For morphometric analysis, negatives were scanned at high resolution and the digitized images transferred to NIH image. A macro was written that enabled us to analyze the distribution of the gold particles: within a given area, the position of each particle was marked and the macro then enabled us to count the particles in contiguous boxes. The size of the boxes was adjustable so that we could analyze the distribution of the particles along the leading edge (not shown), or across the leading edge. Typically boxes of 2 um wide were run at 0.1 um steps into the leading edge, starting outside the cell (Figure 5E). Two different sizes of particles could be analyzed simultaneously on the same image; this allowed direct colocalization of actin and Arp2/3 on the same image, with the same reference for the membrane. Since the cells were triton-permeabilized and exogenous actin had polymerized onto preexisting filaments, membrane position was assigned as the external edge of the dense filament network at the leading edge. This was more easily and reproducibly done at low magnification (see Figure 4).

i) Analysis of the distribution of the nucleation sites and/or Arp2/3 complex (Figures 6A, 9 and 10): consecutive boxes of 2 x 0.1 um were drawn at the leading edge from the outside to the inside of the cells (example in Figure 5E) and the number of particles in each box was plotted as a function of the distance of the box from the membrane.

ii) Analysis of the filament density at the leading edge (Figure 6B): 5 lines were drawn perpendicular to the membrane at the leading edge, and the filaments crossing the lines were marked. The macro described above was then run with 0.1 um steps along the lines and the total number of filaments crossing each of the five lines was counted in each 0.1 um interval.

iii) Analysis of filament parameters (distance between filament intersections and filament length, Figure 8): the measurements were done using the standard length feature in NIH Image. Since most of the actin network at the leading edge is within a single plane (only a small

proportion of the filaments are growing perpendicular to the lamellipod), the tracings and corresponding measurements were done in 2 dimensions only as shown in Figure 7G. For filament length measurements, filaments growing radially from the edge were chosen because of their easily identifiable free end, and they were followed inside the network up to their origin, which was usually at the intersection with another filament (see Figure 7G, panel 1). Occasionally (less than 10% of the total filaments analyzed), some filaments with distinctive origin and end within the network were included in the analysis (Figure 7G, panel 2). The distance between filament intersections was measured as the flat distance between two unequivocal intersections in the actin network within 1-1.5 um at the leading edge. The F-actin concentration at the leading edge was calculated from the total length of filaments within a 1 x 1 um square at the leading edge, assuming a thickness of 176±15 nm for the lamellipod in that particular zone (F. Lanni, personal communication), and a monomer size within the filament of 2.75 nm (46).

RESULTS

Part 1: Relationships between Arp2/3 complex and the barbed ends of actin filaments at the leading edge of carcinoma cells after EGF-stimulation.

Distribution of actin, actin nucleation sites and Arp2/3 complex

MTLn3 cells stimulated with EGF undergo a broad lamellipod extension, which is maximal within 3 minutes and is driven by actin polymerization at the leading edge (27,34). In this study, we have used this well characterized model to investigate the relationship between sites of actin polymerization and Arp2/3 complex location at high resolution in leading edges. We have used three different antibodies raised against three different subunits of the Arp2/3 complex (Arp3, p21, and p34) to analyze the distribution of the Arp2/3 complex in these cells. These antibodies have been previously characterized in fibroblasts (40), but not in tumor cells. We thus first analyzed the localization of the Arp2/3 complex in MTLn3 cells in reference to the actin distribution. Since these anti-Arp2/3 complex antibodies all require methanol fixation, which alters phalloidin binding, actin was visualized in the cells using anti-actin antibodies. The pattern obtained for actin using anti-actin antibodies was virtually identical to the F-actin pattern revealed by fluorescent-phalloidin labeling (data not shown). Immunofluorescence analysis shows that the Arp3 and p21 subunits of the Arp2/3 complex colocalize with actin at the leading edge of these stimulated cells (Figure 1A). P34 showed a similar distribution, although the signal was somewhat weaker (data not shown). None of the proteins was shown to bind strongly to stress fibers, though occasional weak staining of stress fibers was noticed with the anti-Arp3 antibodies (data not shown and Figure 3, EGF3). Some cytoplasmic staining was also observed, including staining in discrete particles that also contain F-actin, as demonstrated by FITC-phalloidin staining (data not shown). The nuclear staining represented mostly non specific binding of the secondary antibodies. Quantitative analysis of the distribution of actin and Arp3 or p21 at the leading edge showed very similar localization, both protein concentrations being maximum within less than one micron at the leading edge (Figure 1B).

We have demonstrated previously that EGF stimulated lamellipod extension is dependent on actin polymerization at the leading edge (27,34). By permeabilizing the cells after stimulation in the presence of 0.45 uM rhodamine-labeled actin, the sites of active nucleation of actin polymerization can be visualized directly (34). Since 0.45 uM is below the critical concentration for the pointed end (47), only free barbed ends are visualized (34,41). Under the current experimental conditions, most of the nucleation activity is localized within less than 2 microns at the leading edge after stimulation (see below). Quantitative analysis of the fluorescence within that specific zone at the leading edge (boxed area in Figure 1A, panel 2) gives an accurate view of the kinetics of appearance of the nucleation sites after stimulation by EGF (Figure 2). Stimulation by EGF generates a transient increase in nucleation activity which peaks very sharply at 50 sec, generating an average 2.4 fold increase in nucleation activity at the leading edge. Nucleation activity is back to residual levels 5-6 minutes after stimulation.

We have done direct colocalization of these active nucleation sites and Arp3 subunit in MTLn3 cells after stimulation (Figure 3). In unstimulated cells (EGF0), Arp3 is enriched in the peripheral submembraneous compartment and, in conjunction with nucleation activity, in ruffling areas. After EGF stimulation (EGF1), Arp3 is recruited homogeneously to the extreme edge of cells in conjunction with newly created nucleation sites (Figure 3, EGF1). After 3 minutes (EGF3), nucleation activity remains confined to the very submembraneous compartment and the tips of the stress fibers (presumably focal contacts). The Arp3 distribution is also mainly restricted to the extreme compartment of the leading edge, but sometimes tends to extend further inside the cell, beyond the nucleation site location. Some particulate staining is also seen is these conditions, and the particles, which contain actin, Arp3 and nucleation sites, appear to be more abundant 1 minute after stimulation (Figure 3, EGF1).

Ultrastructural characterization of actin nucleation activity at the leading edge

The results above showed that Arp2/3 complex and nucleation sites colocalize at the leading edge and in cytoplasmic particles, but the resolution of light microscopy (~0.3 um) was

not sufficient to determine if Arp2/3 complex and free barbed ends overlap in the leading edge. To study at high resolution the distribution of the nucleation sites at the leading edge of lamellipods of stimulated cells, as well as their spatial and temporal relationship with the Arp2/3 complex, we adapted the protocol used to visualize nucleation sites at the light microscope level and used biotin-labeled actin to visualize nucleation sites at the electron microscope level. We have studied the leading edge where the lamellipod is flat enough to allow unequivocal identification of actin containing structures relative to the plasma membrane. To obtain a comprehensive view of the ultrastructure of the cytoskeleton at the leading edge independent of technique-specific artifacts, we used both negative staining and rapid freezing, freeze drying and rotary shadowing (FDS) techniques. The kinetics, amplitude and localization of the nucleation activity obtained with these techniques were strikingly similar to those measured at the light microscopy level, as well as highly reproducible (data not shown).We used only a light permeabilization (low detergent concentration and short extraction time), so that extraction was minimal, and we have shown that under such conditions, even omitting the exogenous actin in the permeabilization step does not affect dramatically the structure of the cytoskeleton at the leading edge (34).

Negative staining images show that the cytoskeleton at the leading edge is arranged as a dense network of filaments (Figures 4 and 5). In unstimulated cells, two types of cytoskeleton organization are found: (a) cell edges in non lamellipodial areas (not organized as leading edges) contain loose networks of long filaments with little, if any, exogenous biotin-labeled actin incorporation (as revealed by the presence of 5 nm gold particles, Figure 5A); (b) typical leading edges of dense filament networks where individual filaments can be seen growing radially from the edge, with some exogenous biotin-labeled actin incorporation (Figure 5B). After stimulation, a large proportion of the cell periphery is arranged as a typical leading edge with a broad peripheral lamellipod extension (see Figures 1, 2 and (33)). The filaments form a denser network of actin where intense biotin-labeled actin incorporation has occurred as a result of the increase in nucleation activity (Figure 4 and 5C). Morphometric analysis of the distribution of the

nucleation sites was conducted using a macro running in NIH Image (see Materials and Methods). With the membrane position set as the extreme edge of the lamellipod as viewed at low magnification (Figure 4), the macro enabled us to count the gold particles in contiguous 2 x 0.1 um^2 boxes from the outside to a few microns inside the cell (Figure 5D). The resulting distribution was then plotted (Figure 6A). On the same negatives, the filament density at the leading edge was evaluated as described in Material and Methods, with the same membrane reference as that taken for the gold particle counts (Figure 6B).

Quantitation of nucleation activity as biotin-actin density at the leading edge confirms a transient increase at 1 min after stimulation, followed by a rapid decrease back to resting levels after 3 minutes (Figure 6A and data not shown). The maximum nucleation activity generated after stimulation is confined within a 0.2-0.3 um zone directly at the membrane, and only residual (background) nucleation activity remains more than 1-1.5 um away from the membrane (Figure 6A). As opposed to the very sharp location and transient generation of the nucleation sites, EGF stimulation results in about a 1.5 fold increase in filament density within a 1.5-2 um zone adjacent to the membrane at the leading edge. This increased density remains for 5 minutes after stimulation (Figure 6B). The maximum nucleation activity generated after stimulation is thus confined to a narrower region than the one covered by the high filament density zone generated after stimulation.

To get greater insight into the 3-dimensional filament architecture at the leading edge, we used the FDS technique. This technique allows a very high resolution of the cytoskeleton with minimum reorganization of the actin filaments, potentially minimizing the generation of artifacts. The results obtained using this technique were entirely consistent with those acquired on negatively stained samples, and the diameter of the filaments observed in the replicas was routinely under 11 nm, indicating a high degree of resolution of the technique. We analyzed the filament architecture at the leading edge of the cells before and after stimulation with EGF. As with negative staining, the leading edge could be identified easily by its typical orthogonal arrangement of filaments with a denser zone at the extreme edge (Figure 7A and C), as opposed

to loose bundles of parallel filaments in other parts of the cells (Figure 7B). The 5 nm gold particle distribution reveals the filaments that have incorporated biotin-actin, localizing the active nucleation sites at the extreme edge of the cells (Figure 7, D and E, and data not shown), as shown previously with negative staining (Figures 5 and 6A). The network of actin filaments was denser after stimulation (Figure 7C), and different types of filament crossing and/or branching were observed (Figure 7F), including: (a) branching with an angle of ~70°, typical of the in vitro branching observed for Arp2/3 complex (48,49) on filaments growing radially at the leading edge or within the network; (b) T-branching inside the network at the leading edge (50,51); and (c) Y-branching and filament branching with smaller angles (50,51). The distance between filament intersections inside the network within 1-1.5 um under the membrane was measured in unstimulated cells (non lamellipodial-type edge: 224±9 nm, n=171; leading edge-type: 142±4 nm, n=253), and in cells after stimulation for 1 min (155±6, n=208) or 3 min (158±5, n=235). To evaluate the concentration of F-actin at the leading edge, the total length of actin filaments was evaluated in a 1x1 um^2 box at the leading edge, and was found to be 66±6 um/um^2. Assuming 176±15 nm for the thickness of the lamellipod at the leading edge (F. Lanni, personal communication), this gave us an approximate concentration of 9.3 mg/ml for F-actin at the leading edge.

We then measured the filament length for the filaments with one free end at the leading edge; the filaments were measured starting from the free end and going back to the origin of the filament (generally at the intersection with another filament, see Figure 7G, panel 1), or in between 2 intersections for filaments where no free end could be found (Figure 7G, panel 2). The filament length distribution within a 1 um zone behind the membrane of resting cells (non lamellipodial-type and typical leading edges combined), is widely distributed, with filaments as short as 30 nm and as long as 1000 nm, most of the filaments being in the range of 100 to 400 nm (Figure 8 A and B). In contrast, after EGF stimulation, the cell perimeter consists mainly of broad lamellipodial structures with typical leading edges with short filaments, ranging from 100 to less than 300 nm (Figure 8C). This particular arrangement of short filaments persists after 3

minutes of stimulation (Figure 8D), consistent with the maintenance of a high filament density (Figure 6B). The average filament length reflects that change, with a mean filament length of 261±15 nm in resting cells versus 179±4 and 189±5 respectively 1 and 3 minutes after EGF stimulation. This results in an average 34% decrease in filament length at the leading edge after 1 minute, and 29% decrease after 3 minutes compared to unstimulated cells (consistent with measurements made on negatively stained samples showing 32 and 28% decrease at 1 and 3 minutes respectively, data not shown).

Spatial and temporal relationships between the nucleation sites and Arp2/3complex

Colocalization of the Arp2/3 complex (Arp3 and p21 subunits) and the nucleation sites was performed on negatively stained samples using the morphometric analysis described above. For each cell, Arp2/3 (10 nm gold particles) and the nucleation sites (5 nm gold particles) were measured on the same image, with exactly the same reference for the position of the membrane (determined as above). The amount of Arp3 at the leading edge approximately doubles 1 min after EGF stimulation and is distributed as a broad peak starting ~100 nm back from the membrane (offset from the nucleation sites, Figure 9). Three minutes after stimulation, the amount of Arp3 at the leading edge is slightly reduced, but is still higher than before stimulation. P21 distribution follows the same trend as Arp3 (Figure 9). After EGF stimulation, p21 is distributed within 1-1.5 um at the leading edge, where it is separated from the peak of nucleation activity by ~100 nm. P21 concentration doubles after 1 minute and the spatial distribution of the protein remains stable 3 minutes after stimulation, with only a slight decrease in the amount of p21 present.

We hypothesized that the offset from the membrane that was observed for Arp2/3 distribution might be due to the growth of the actin filaments from exogenous actin that we use to visualize the active nucleation sites. We thus designed an experiment where we could prevent actin polymerization, while still labeling the barbed ends using biotin-labeled gelsolin-actin complexes. As shown in Figure 10, under these conditions the edge of Arp3 distribution now

aligns perfectly with the position of the nucleation sites at the membrane. Interestingly, the fact that the distribution of the nucleation sites is slightly offset after treatment with gelsolin suggests that most of the barbed ends are oriented toward the membrane as previously reported for resting fibroblasts (52-54).

PART 2: Generation of MTLn3 cells expressing talin antisense mRNA

Characterization of talin expression

Initial selection for MTLn3 cells that had stably incorporated the antisense vector made use of the hygromycin resistance marker present on the pBPSTR-1 plasmid. Cells were transfected using the lipofectamine procedure and then grown in medium containing hygromycin and tetracycline (to suppress expression of the antisense construct during the selection process). Individual hygromycin resistant clones were generated and then grown in the presence and absence of tetracycline for 3 days in order to determine the degree of suppression of talin expression. Cell extracts were then analyzed by Western blotting to quantitate the reduction in amount of talin protein (Figure 11). A clone (termed Clone 10) was identified that showed roughly 50% reduction in talin expression when grown in the absence of tetracycline compared to growth in the presence of tetracycline - labeled T1C10 and T1C5 (Figure 11). This clone was then utilized for analysis of focal contacts and EGF-stimulated lamellipod extension.

Focal Contacts are altered in Clone 10 Cells.

Focal contacts were analyzed in Clone 10 cells after stimulation with EGF. The cells were grown in the presence or absence of tetracycline in order to repress or allow (respectively) expression of talin antisense RNA. Paired images of talin localization and F-actin are shown in Figure 12. MTLn3 cells and Clone 10 cells grown in tetracycline show typical elongated focal contacts when stained with anti-talin antibodies (top row, left image of each pair). The F-actin stain indicates that stress fibers terminate in these focal contact areas.

Clone 10 cells grown in the absence of tetracycline show a remarkable reduction in talin staining in focal contacts. This correlates with an overall decrease in the number and staining of stress fibers. The images shown are of cells fixed 3 minutes after stimulation with EGF. There is still staining for F-actin at the periphery of the cells, together with staining for talin in those areas. That suggests that the reduced talin concentration present in the Clone 10 cells may result in a loss of talin from cell-substratum adhesion sites, prior to its loss from EGF-stimulated actin polymerization sites.

Lamellipod extension is roughly normal in Clone 10 cells

MTLn3 and Clone 10 cells were grown in the presence or absence of tetracycline and then stimulated with EGF and lamellipod extension measured as increases in area (Figure 13). MTLn3 cells show an increase in area reaching a maximum 5 - 6 minutes after addition of EGF. Clone 10 cells grown in the presence of tetracycline show a somewhat smaller peak 4 minutes after stimulation, while Clone 10 cells grown in the absence of tetracycline (conditions of reduced talin expression) may show a slight delay in lamellipod extension. However, with the limited sample sizes currently utilized, it is unclear that either of the Clone 10 measurements is significantly different from the MTLn3 cell responses.

DISCUSSION

Part 1: Relationships between Arp2/3 complex and the barbed ends of actin filaments at the leading edge of carcinoma cells after EGF-stimulation.

Organization of the leading edge of cells after stimulation

The general organization of the actin cytoskeleton in carcinoma cells resembles closely what has been described previously for chemotactic amoeboid cells such as macrophages (51), leukocytes (55) and *Dictyostelium discoideum* (52,56,57). Although the extreme edge of the cell has some features comparable to what has been described for constitutively moving cells such as keratocytes (58), the general organization of the actin cytoskeleton in rat adenocarcinoma cells is different. In unstimulated cells, the cytoskeleton at the edge of the cell is arranged as a network of long filaments, occasionally in bundles parallel to the edge. When such cells do have a leading edge, the filaments in that particular area are arranged in a 1-1.5 um wide high density orthogonal network at the edge, very similar to the leading edge of unstimulated fibroblasts (52,54,58,59). The density of the filaments then rapidly decreases a few microns away from the edge. After stimulation, the density, as well as the width of the high density network at the edge, increases, and a clear zone mostly devoid of actin filaments is created behind the leading edge as the lamellipod advances, features that are not observed in keratocytes (58,60). The network at the leading edge is composed of tightly entangled interwoven filaments, featuring multiple intersections of two or more filaments. The complexity of the network is increased after stimulation as the filament density increases. The filaments before stimulation appear to be relatively short (0.2-0.3 um), and they get even shorter (<0.2 um) after stimulation as the network becomes increasingly denser. This is slightly shorter than previously reported filament lengths measured on quick-frozen deep-etched macrophages samples (0.5 um, (61), or inferred from depolymerization kinetics in leukocytes (0.3 um, (62), but is remarkably similar to what has been measured in stimulated platelets (0.1-0.3 um; (45) or in *Dictyostelium* where the mean filament length was 0.2 um with a large proportion of small (<140 nm) filaments (57,63). Comparison of

negative staining and FDS to detect artifacts particular to specimen preparation showed a clear consistency between the measurements made on negatively stained samples and those made on rotary shadowed samples.

It has been shown recently that the Arp2/3 complex can generate an angle of 70° between filaments in vitro (48). That type of branching has been observed in the cytoskeleton of keratocytes (58), and it has been suggested that Arp2/3 could be a major component of the organization of the cytoskeleton in vivo, by creating filament branching (49,64). Although we have noticed some 70° branching at the leading edge of MTLn3 cells, the organization of the cytoskeleton that we observed is again more typical of what has been described in chemotactic amoeboid cells where a more complex set of branching was observed, including T- and Y- and X-branching as well as 70° branching (51,55,56). This T, Y, and X morphology does not appear to be technique dependent, but rather common to chemotactic cells as seen by different techniques such as critical point drying (51,65), FDS (this study and (51)) or negative staining (this study and (54). Furthermore, the 3D architecture of the cytoskeleton at the leading edge, as well as the distance between filament intersections and the actin concentration that we measured at the leading edge, are consistent with a network of actin and filamin-type crosslinkers (50,66). Thus, although we can not rule out that the Arp2/3 complex might have a role in crosslinking the filaments, other molecules have been described, particularly among the filamin family, such as ABP280 and ABP120, that are known to have a crucial role in maintaining the integrity of the cytoskeleton and in defining filament branching at the leading edge (56,67). The relative contributions of these molecules to filament organization might differ from one type of cell to the other, which could explain why a 70° Arp2/3 branching pattern is more common in the keratocyte (58). Alternatively, Arp2/3 branching might be more involved in constitutive movement, as shown in keratocytes, as opposed to transient and rapid reorganization of the cytoskeleton after EGF stimulation.

EGF stimulation triggers a transient increase in nucleation activity which is tightly controlled in terms of kinetics (sharp peak at 50-60 sec) and localization (within only 100-200

nm at the extreme edge of the lamellipod). The position of the nucleation sites remains constant with respect to the membrane of the extending edge as the cells form lamellipods. Most of the filaments growing at the leading edge are arranged radially from the extremity of the lamellipod, parallel to the main axis of growth, but some filaments also grow perpendicularly to the network. The increase in nucleation activity after stimulation is accompanied by an increase in filament density at the leading edge covering a zone of dense actin network extending up to 2-2.5 um further inside the cells. As the filament density increases after stimulation, we have noticed a decrease in mean filament length and a loss of long (>300 nm) filaments. The most likely explanation for that would be the intervention of severing activity turned on by EGF stimulation (see below), or de novo nucleation, but it is inconsistent with a simple uncapping event. However, uncapping could be the mechanism responsible for generating nucleation sites that we see at the ends of the stress fibers, since the growth happens only at the extreme ends of the stress fibers (i.e. not consistent with severing) and does not seem to involve any Arp2/3 complex recruitment.

Spatial and temporal regulation of the Arp2/3 complex

Both light and electron microscopy show that the Arp2/3 complex is localized within 1.5-2 um at the leading edge, where its concentration is increased after EGF stimulation. Although a subset is present at the membrane precisely where the nucleation sites are, the distribution of the Arp2/3 complex is not restricted to the 100-200 nm polymerization zone at the membrane, but extends further inside throughout the dense F-actin network both before and after stimulation. The increase in Arp2/3 concentration directly at the membrane follows approximately the increase in nucleation activity. Both show a 2-2.5 and 1.2-1.5 fold increase respectively at 1 and 3 minutes after EGF stimulation. At 1 minute after stimulation, the Arp2/3 concentration is maximum at the membrane and decreases back to the level measured in unstimulated cells within a distance of 2 um from the growing edge, which corresponds exactly to the site where the membrane was before stimulation (since the lamellipod has extended 2.2 um at 1 minute and 5.2

um at 3 minutes after stimulation, data not shown). We thus propose that the Arp2/3 distribution that we observed at 1 minute is the result of the accumulation of Arp2/3 at the membrane as the leading edge advances: Arp2/3 is recruited at the membrane concurrently with the increase in nucleation activity but, as opposed to the nucleation sites that remain at the membrane as it moves, the Arp2/3 complex stays with the actin filaments as the leading edge advances. This suggests that Arp2/3 is functioning as a pointed end capper, which would explain the broad peak of Arp2/3 distribution compared to the sharp peak of nucleation sites at the leading edge. It implies that Arp2/3 molecules would have to be recruited to the submembraneous compartment from the cytoplasm, either by facilitated transport, diffusion (68) or mRNA targeting. The particles of Arp2/3 and actin that are identified in the cytoplasm of the cells back from the leading edge could be important players in this transport/recruitment process of Arp2/3 complex after stimulation.

Interaction of Arp2/3 and the nucleation sites at the leading edge

The Arp2/3 complex caps the pointed ends of actin filaments with high affinity (64). Could then the Arp2/3 complex have only a passive role of pointed end capping at the leading edge? In this model, the increase in Arp2/3 concentration that we observe at the leading edge after stimulation could simply reflect the increase in pointed ends that has been measured (34), favoring a severing mechanism that could generate both new barbed ends and new pointed ends. The Arp2/3 distribution, however, does not follow exactly the filament distribution as it tends to increase more than the filament number does and drops more abruptly than the filament density within 2 um of the leading edge. Thus, while we can not rule out from our data a simple pointed end capping role for Arp2/3, it seems likely that the complex has a more active role in actin polymerization.

Altogether, the increase in the number of pointed ends observed after stimulation (Chan et al., 1998) as well as the decrease in filament length and disappearance of the long filaments, rule out uncapping as the dominant mechanism for generating the increase in nucleation activity

observed after EGF stimulation. The two other mechanisms capable of generating new nucleation sites after stimulation would be either de novo nucleation or severing (or both combined). Both mechanisms could account for the decrease in filament length that we observed, the former because it might generate a large population of filaments that will be shorter than the preexisting ones, and the latter because it actually cuts the preexisting filaments into smaller ones. It should be noted, however, that the disappearance of the longer filaments that we observed immediately after stimulation is highly suggestive of a severing mechanism. Original work on the Arp2/3 complex suggested that it could nucleate actin polymerization at the surface of the bacteria *Listeria Monocytogenes* (69). More recent data, however, indicate that the Arp2/3 complex is probably not a true nucleator but rather captures and stabilizes unstable actin dimers (48). The rate constants of assembly/disassembly of actin monomers into a dimer are such that the probability of generating actin dimers from free monomers or monomers bound to sequestering proteins in vivo is essentially null. Similarly, the formation of a complex between Arp2/3 and one actin monomer, as well as addition of a second actin monomer to this complex to create a nucleus is extremely unlikely (Figure 14). Capture and stabilization of actin dimers or oligomers by the capping of pointed ends by the Arp2/3 complex is however a very efficient process that can lead to the stabilization of nucleation sites for actin polymerization. We propose then that a severing activity is taking place after stimulation to rapidly generate actin oligomers that are stabilized by the Arp2/3 (Figure 14). Such a severing activity is, besides, entirely consistent with our data showing a decrease in the mean length of the filaments at the leading edge, as well as a disappearance of the long filaments after stimulation. A likely candidate for this severing activity would be cofilin, which generates free barbed ends by severing and has been proposed as a major component in generating nucleation activity after stimulation (70-74).

Based on these results, we present a modified version of the model proposed by Mullins et al. (48) for the generation of nucleation sites at the leading edge that drives the extension of the lamellipod. As shown in Figure 14, EGF stimulation triggers a signal that transiently and

locally turns on cofilin activity at the leading edge. The actin filaments are severed, generating small actin oligomers free both at their pointed ends and barbed ends. Concomitantly, Arp2/3 is recruited from the cytoplasmic pool and targeted to the leading edge, where it can then stabilize these oligomers by binding to their pointed ends before they completely depolymerize. These stable nuclei then polymerize transiently and rapidly until their barbed ends are capped by capping protein (not shown). While in this model the Arp2/3 complex does not need to be specifically "activated" locally, we can not rule out the intervention of molecules that would act in synergy with the complex to promote its ability to bind oligomers and nucleate actin filaments (75). Once the filaments have polymerized, the final 3 dimensional structure of the leading edge will be achieved by crosslinking by both branching due to the binding of the Arp2/3 complex to the side of the filaments and intervention of other crosslinkers like filamins to stabilize the filament network (not shown). The Arp2/3 complex would thus be one of the major players at the leading edge, by acting concurrently on the actin cytoskeleton through the 3 different mechanisms that have been identified *in vitro*, i.e. stabilizing actin nuclei, capping the pointed end and forming branching networks (48). The question remains, however, as to what is the mechanism by which cofilin and Arp2/3 complex are targeted to the leading edge, and further work is required to decipher the sequence of molecular interactions that lead to actin polymerization and leading edge advance.

PART 2: Generation of MTLn3 cells expressing talin antisense mRNA

Our preliminary analysis of cells stably transfected with a talin antisense vector indicates :1) talin expression can be suppressed roughly 50%, 2) focal contact formation is perturbed when talin expression is reduced, and 3) lamellipod extension is not strongly affected. The 50% reduction in talin expression is roughly similar to what has been reported by Western blotting using an antisense vector in fibroblasts (76). Those investigators also reported a clear decrease in focal contacts and stress fibers. Our results indicate that lamellipod extension is not as strongly perturbed as focal contact expression. This may be due to the remaining talin present in the cells

(50% of control). Immunofluorescence images show talin still present in the leading edges of cells stimulated with EGF, consistent with the induction of lamellipod extension.

The selective reduction in focal contact and stress fiber formation in Clone 10 cells grown in the absence of tetracycline may result in reduced adhesion to the substratum. Interference reflection microscopy (33) could evaluate overall formation of focal adhesions to the substratum. Detachment assays (77,78) could determine directly cell adhesiveness to various substrata. An inability to form strong adhesive contacts could inhibit cell movement in response to chemotactic stimuli. It could also affect the ability of cells to metastasize, either through inhibition of chemotactic movement or through blocking the ability to adhere to sites in target organs for metastasis. In the event that the talin antisense transfectants show perturbations in adhesion or chemotaxis, a test of the metastatic capability of these cells would address whether there is a correlating affect on metastasis. For a more accurate evaluation of the stage during the metastatic process that is affected, new assays for evaluating the in vivo distribution of cells during metastasis must be developed. We have submitted a proposal to address this important question.

CONCLUSIONS

Mechanisms of metastasis of tumor cells rely upon cell movement and protrusive activity (e.g., (4)). Thus a molecular understanding of amoeboid chemotaxis in metastatic cancer cells may identify new targets for therapeutic intervention. The rat mammary adenocarcinoma cell line MTLn3 provides a number of advantages for such studies(79). These cells grow easily in tissue culture and, when injected into the mammary fat pad of syngeneic Fisher 344 rats, form first a primary tumor and then lymph node and lung metastases. MTLn3 cells express roughly 50,000 EGF receptors per cell, while a nonmetastatic derivative termed MTC from the same original tumor does not express EGF receptors(28). Expression of the EGF receptor in the MTC cells increases metastatic ability without affecting primary tumor growth rate(80). This result combined with the literature correlating expression of EGF receptor family members with poor prognosis for cancer patients (13,16,81) highlights the potential usefulness of analyzing chemotactic responses to EGF.

The lamellipod is essential for chemotaxis

Chemotactic responses of MTLn3 cells assayed with microchemotaxis chambers are highly sensitive to cytochalasin D, an inhibitor of actin polymerization(27). Nocodazole, an inhibitor of microtubule polymerization, is much less effective in inhibiting chemotaxis in response to EGF, even at concentrations which block cell division. Thus, studies of EGF-stimulated motility in MTLn3 cells have focused on the regulation of actin-based structures, consistent with previous studies of amoeboid chemotaxis in a large number of systems.

A number of different actin-based protrusions can be involved in chemotactic responses (82). Filopodia are long, thin fiber-like projections from the cell distinguished by the presence of an ordered array of parallel actin filaments covered by the plasma membrane(83,84). In both neurons and amoeboid organisms such as *Dictyostelium*, filopodia may play a role in sensing spatial gradients of soluble and matrix-bound molecules(85). In *Dictyostelium*, the major form

of cell translocation utilizes the projection of pseudopods(86). Pseudopods are large cylindrical or tubular structures which form rapidly and often project off the surface of the dish. They comprise a dense crosslinked meshwork of actin filaments. However, neither filopods nor pseudopods are characteristic of MTLn3 cell motility. As seen in Figure 15, protrusion of the cell towards the micropipet was mainly in the form of a broad, flat lamellipod. Lamellipods are roughly two dimensional cell protrusions in which the width and depth can be 10 times as large as the height(58,60,87). They project parallel to the substratum upon which the cell is moving. As with pseudopods, lamellipods also contain a meshwork of crosslinked actin filaments. The difference in morphology between pseudopods and lamellipods may be due to the types of crosslinking proteins present (30,88) or the organization of actin polymerization sites. Another common protrusion is a more vertically oriented sheet containing F actin. In locomoting fibroblasts(89,90) and MTLn3 cells, these structures, termed ruffles, arise from lamellipods which are extended, do not attach, and then rise up and are brought back over the dorsal surface of the cell as a ruffle. The ruffle then disappears, being resorbed into the cell body. Thus in randomly locomoting fibroblasts and MTLn3 cells, it appears that ruffles result from lamellipod retraction. In systems in which expression of activated rac produces increased ruffling, it is important to evaluate whether this reflects increased lamellipod extension, decrease lamellipod adhesion, increased myosin induced lamellipod retraction, decreased rates of resorption of ruffles, or formation of vertical projections directly.

The micropipet assay has been useful in demonstrating the morphology of actin structures induced by chemoattractants which bind to G protein coupled receptors(91,92), receptor tyrosine kinases(33), and extracellular matrix molecules(93,94). Genetic analyses of signaling are particularly well advanced in *Dictyostelium* (95-97)and *S. cerevisiae* (98,99). Remarkably, the time scales of these responses range from under a minute (for *Dictyostelium*) to several hours (for *S. cerevisiae*). The form of the protrusion utilized by *Dictyostelium* for motility, the pseudopod, may be necessary for the relatively high speed of movement of these cells. On the other hand, in *S. cerevisiae* , motility is dependent on gene transcription and a remodeling of the cell wall which

requires hours. For cells utilizing extracellular matrix receptors and receptor tyrosine kinases, the speed of protrusion is intermediate - and the corresponding actin regulatory mechanisms may be most effective in generating lamellipodial type structures.

To determine the actin-based structures which are most relevant to chemotactic responses, it is necessary to directly view cells undergoing chemotactic responses. Boyden and microchemotaxis chambers do not provide that opportunity, being end point-based assays which provide information regarding the number of cells that have crossed a membrane rather than how they cross the membrane. The chemotactic responses of individual cells can be examined in detail using micropipets to directly stimulate individual cells with a spatial gradient of EGF while following their movement(33). In Figure 15, the pipet was originally placed at the rear of the cell, but even during the time necessary to adjust the pipet placement, the cell began reorienting towards the pipet. The cell then moved fairly directly towards the pipet, undergoing continuous protrusion at the front and retraction at the rear. When the pipet was moved, reorientation of the cell to follow the pipet was clear within 2 minutes, providing direct evidence that EGF is a true chemoattractant for MTLn3 cells. Detailed time lapse video analysis showed that this change in direction involves redirection of the major axis of the lamellipod, using preexisting structures that become more active. However, in other cases, position of the pipet at the rear of a clearly polarized cell result in a complete reversal of cell polarity than does not involved any turning of the leading lamellipod.

Initiation and growth of the lamellipod

Given that chemotactic responses to EGF can be mediated by lamellipod extension, the process of lamellipod extension has been explored in more detail. An advantage of using EGF to stimulate lamellipod extension is that bath application of EGF stimulates synchronous production of lamellipods on large numbers of cells (Figure 16). Up to 90% of the cells on the dish produce lamellipods which are fully extended by 3 - 5 minutes after addition of EGF. The lamellipods tend to be extended from the edges of the cell, with less extension occurring from

regions that were rounded or less well spread. The morphology and placement of the lamellipod depends upon the attachment status of the cell. Cells which are recently plated or poorly spread do not show EGF stimulation of lamellipods parallel with the substratum. Rather, they display randomly oriented projections. In the most extreme case of cells in suspension, these projections can occur over all regions of the cell surface (Figure 17). These results contrast with studies of EGF-stimulated responses in other cell types. For example, stimulation of NR fibroblasts (100)or A431 cells (101,102)with EGF typically results in ruffling and cell retraction.

By utilizing conditions under which the lamellipods are flat and extended parallel to the surface of the substratum this system is optimal for the analysis of temporal and spatial localization of specific proteins during chemoattractant-induced responses. The first question being addressed is the role and location of actin polymerization. Consistent with the sensitivity of chemotaxis to inhibitors of actin polymerization, lamellipod extension is also inhibited by low concentrations of cytochalasin D and not by nocodazole. This indicates that actin polymerization is a necessary condition for extension of lamellipods. To determine the site of actin polymerization, cells were stimulated with EGF and then briefly permeabilized and exogenous, rhodamine- or biotin-labeled actin was allowed to polymerize onto the sites of actin polymerization. The exogenously added actin was then visualized by light (34) and electron microscopy (Figure 18). Light microscopy localizes the growth of actin filaments to the leading edge of lamellipods almost exclusively, with little polymerization associated with the end of the stress fibers (34).At the EM level there is a clear localization of actin polymerization to within 200 nm of the expanding edge of the lamellipod. This suggests that there is a highly localized site at which stimulation of actin polymerization is occurring. This site is likely to be extremely close to the plasma membrane. However, note that the lamellipod is only about 200 nm high. The actin cytoskeleton of the lamellipod is therefore in close contact with the plasma membrane on its lower and upper surfaces (which extend several 1000 nm towards the cell body) as well. Nevertheless, actin polymerization sites are most concentrated directly at the growing edge of the lamellipod extension.

Each actin filament is an oriented double helix consisting of a fast growing barbed end and slow growing pointed end (so named by the electron microscope images generated by myosin decoration of actin filaments). In vivo, conditions are typically such that growth occurs from free barbed ends and depolymerization occurs from the pointed ends(30,103,103,104). Thus proposed mechanisms for generating actin polymerization sites involve increases in free barbed ends of actin filaments. At least 3 different mechanisms might account for the generation of free barbed ends, i.e. de novo nucleation, severing or uncapping(35). A number of different proteins have been identified that can facilitate such mechanisms. Although the in vitro biochemistry of the proteins involved is well characterized (30,88,105,105), most of the results reported have been rather inconclusive or contradictory as to which of these mechanisms may be pertinent in vivo. Depending on the cell type, different mechanisms may be dominant or several might operate together to optimize the generation of barbed ends.

For de novo nucleation, filaments are polymerized from a nucleus created by the assembly of 3 G-actin monomers. While some molecules are known to facilitate the assembly of such nuclei in vitro(38,75), by decreasing the lag phase that characterizes actin polymerization from pure G actin in vitro, definitive evidence for the intervention of this mechanism in vivo is still lacking. A protein that might facilitate this mechanism is the cytoskeletal molecule talin which, in addition to being a major component of the focal contacts (106), has consistently been found in the cortical microfilament web of ruffling membranes and extending lamellipods (107-109). Further data suggests that talin might have a specific function at the leading edge where it is required for cell spreading and migration (76,110). Since talin can bind actin in vitro and promotes the nucleation of actin filaments (38), it may also nucleate actin filaments in vivo, which would account for its role in cell motility. More recently, the Arp2/3 complex has been identified as a good candidate for nucleation of actin filaments in vivo. Originally identified from the cortex of Acanthamoeba (111), it has been shown to be evolutionarily conserved and generally associated with regions of dynamic filament assembly in organisms ranging from Acanthamoeba to mammalian fibroblasts (40,112,113). Furthermore, the Arp2/3 complex can

specifically induce actin polymerization and nucleation at the surface of Listeria monocytogenes(69) a bacterium whose motility in the cytoplasm of mammalian cells is a model for mammalian cell protrusive ability (114,115). In vitro data suggest that the Arp2/3 complex alone is not be a true nucleator (116), but it has been shown to rapidly nucleate actin filaments in combination with the Listeria ActA protein (75). Although this mechanism might explain Listeria motility, the identification of the mammalian equivalent of ActA is necessary to prove that a similar mechanism operates during lamellipod extension. An alternative function of the Arp2/3 complex might be to capture and stabilize actin dimers or small oligomers generated by other mechanisms such as severing, or to act simply as a pointed end capping protein.

A number of different proteins have been characterized as having a severing activity in vivo as well as in vitro. However, to generate a large number of barbed ends by severing, the severing protein must not remain bound to the resulting filament end. Such a behavior has been described for the cofilin family of severing proteins, including cofilin, ADF (Actin Depolymerizing Factor) and destrin (74,117,118). Cofilin is an essential actin-regulating protein widely distributed in all eukaryotes. Its depolymerization/severing activity is pH dependent. Overexpression of cofilin in cells induces increases in number of actin filaments suggesting that the severing activity rather than the actin-depolymerizing or monomeric actin-sequestering activity is physiologically significant in vivo(119). The activity of cofilin is regulated by its phosphorylation status, the phosphorylated form being unable to bind actin. Chemotactic peptides and phorbol 12-myristate 13-acetate (PMA) in neutrophils, as well as growth factors in epithelial cells induce a dephosphorylation of cofilin which is associated by a shift of cofilin to F-actin rich areas in the cell periphery, suggesting that cofilin could be a major component in generating nucleation activity after stimulation (70-73). A kinase that turns off cofilin activity has recently been identified as LIMkinase-1 (120,121). It is possible that LIMK-1 lies on a pathway activated by the small GTP-binding protein rac. It is interesting to note that if inhibition of cofilin (an actin severing protein) is the mechanism of action of rac, this would suggest that the lamellipodia and ruffles seen in cells expressing activated forms of rac may reflect a reduced

rate of turnover of spontaneously induced protrusions, rather than an increase in the rate of initiation or nucleation of actin polymerization.

Finally, numerous molecules are present within cells that can act as capping proteins for barbed ends or pointed ends, and a simple uncapping of the barbed end could be a rather straightforward mechanism to generate nucleation sites. In neutrophils, for example, two major calcium-dependent capping proteins(gelsolin and capG), and one calcium-independent capping protein with a high affinity for filament ends (the non-muscle isoform of capZ), are present in large amounts (122). In Dictyostelium, the capping protein cap32/34 accounts for the major Ca2+ insensitive capping activity (35). In erythrocytes, adducin acts a barbed end capper that is down regulated by calmodulin in presence of calcium (123,124). Studies on permeabilized platelets (32) and neutrophils (125) favored an uncapping mechanism to account for GTPγS-stimulated nucleation activity. In Dictyostelium, capping protein is released from barbed ends by PIP2 in vitro, suggesting a mechanism for regulation of uncapping (126). However, uncapping mechanisms predict an increase in filament length following stimulation, while studies in platelets, as well as in neutrophils (62) fail to report any increase in filament length and consistently show an increase in filament number incompatible with a pure uncapping mechanism. Furthermore, capZ appears to be recruited to the cytoskeleton after stimulation, instead of leaving the cytoskeleton as would be predicted by an uncapping mechanism for barbed end formation (36). In total, these studies suggest that although capping proteins undoubtedly have a major role in the control of the cytoskeleton, that role might be to terminate rather than stimulate actin polymerization.

The real mechanism for the generation of barbed ends may be a combination of the 3 different processes described above. Combined models would also integrate actin-interacting proteins that serve many functions such as gelsolin and profilin. Gelsolin is a calcium-regulated actin-binding protein that regulates actin assembly by severing, capping and nucleating filaments. For severing to occur, both actin and gelsolin undergo large conformational changes (127). In fibroblasts, gelsolin is an essential effector of rac-mediated actin dynamics, acting

downstream of rac recruitment to the membrane, though the exact role of gelsolin in the pathway is still unclear (128). Indeed, gelsolin-null cells are only partially defective in lamellipod extension, ruffling response to serum or EGF stimulation and motility (64), and other data suggest that the pathway that leads to growth factor-activated lamellipod extension might involve phosphatidyl inositol bisphosphate (PIP2)-mediated uncapping of the barbed ends through direct PI-3 kinase activation by rac (Carpenter et al, 1997). In addition, PLC-gamma activation and mobilization of gelsolin from a plasma membrane bound state are required for EGFR-mediated fibroblast motility (129). In neutrophils, activation of rac by G-protein-coupled receptors triggers the dissociation of actin-gelsolin complex, independently of PI3kinase (130), and this is accompanied by gelsolin translocation from the soluble pool to the cytoskeleton (131). Similarly, in platelets, thrombin stimulation activates the rac pathway leading to lamella and filopodial extension through uncapping of gelsolin from the barbed ends of filaments, also independently of PI-3 kinase but through an increase in PIP2 (Hartwig et al, 1995). Since PIP2 is known to inhibit actin filament severing and capping by gelsolin in vitro (Hartwig et al, 1996), the dominant gelsolin activity in vivo might be capping of the barbed ends rather than severing. Profilin, a ubiquitous 12 to 15 kDa protein, is also multifunctional, and may contribute to sequestering monomeric actin, accelerating nucleotide exchange on actin monomers, decreasing the critical concentration of the barbed end of actin filaments, and promoting polymerization when barbed ends are free(132-134). Profilin forms a complex with actin, named profilactin, which caps the barbed ends of the filaments. Purified profilin does not have this effect. This complex can be dissociated by PIP2, thus participating in the generation of nucleation sites by uncapping barbed ends (135,136). When barbed ends are capped, profilin simply sequesters globular actin (137). Along with gelsolin and profilin, a number of other molecules that interact with actin are regulated by PIP2. Thus, in addition to serving as a precursor for diacylglycerol and inositol trisphosphate in signal transduction cascades (138), PIP2 may promote actin filament growth by 2 potential mechanisms: inhibiting capping, or removing capping proteins from barbed ends , since it interacts directly with cytoskeletal proteins such as talin, gelsolin, capping protein and

profilin (135,139). The severing of PIP2 by PLC's may trigger activation or inhibition of actin polymerization via these mechanisms.

Given that free barbed ends are generated, what are then the forces that generate the protrusion? Protrusion can be generated in at least two different ways: 1) through the pressure of the newly polymerizing actin filaments directly on the plasma membrane (termed the Brownian ratchet mechanism(140)), or, 2) through osmotic expansion of the actin meshwork (the gel osmotic mechanism(30)). Another possibility, that myosin based contraction would push the actin filaments outwards and thus extend the lamellipod seems less likely, since such a mechanism (in its simplest form) should not require actin polymerization, and also would be unlikely to require actin polymerization directly under the extending membrane(141). An alternative version of a myosin-based mechanism would have myosin contraction continuously pulling newly polymerizing actin filaments away from the leading edge, creating a cortical flow towards the nucleus. Protrusion could then occur if the actin meshwork were arrested by attachment via extracellular matrix receptors to the substratum, freezing the rearward flow and the continued polymerization of filaments then causing protrusion of the edge of the cell. This mechanism appears to be important in growth cone dynamics(142).

Interactions with the substratum could be important either for anchoring filaments to generate protrusive force or to regulate the site of actin polymerization. Focal complexes have been identified at the leading edge of projections induced by activated rac(109). Such complexes could occur in regions which have just established contact with extracellular matrix and thus generate preferred sites for actin polymerization, given the extremely flat nature of the lamellipod and its proximity to the matrix surface. As the lamellipod extends, new regions of plasma membrane which bind to extracellular matrix molecules extending off the surface might trigger continued growth of the lamellipod. This does not appear to be the case for EGF-stimulated lamellipod extension in MTLn3 cells(33). EGF-stimulated lamellipod extension still occurs either in the presence of RGD peptides which block cell attachment or over nonadhesive surfaces. In Figure 19, cells were plated on patterned coverslips containing 10 μm wide adhesive

stripes. Although the cells attached and were elongated due to the pattern of adhesivity, EGF-stimulated lamellipod extension still occurred over the nonadhesive regions. Thus, adhesion of the focal complexes to the substratum is not required for the extension of the lamellipod. This distinguishes stimulated lamellipod extension from processes such as cell spreading, which require an adhesive surface. However, interaction with an adhesive surface was necessary for stabilization of the lamellipod, as described in the next section.

Stabilization of the Lamellipod

Following extension of the lamellipod, two extreme outcomes are possible. One is that the lamellipod remains in place, the other is that it is retracted. As shown in Figure 19, this depends upon the ability of the cell to adhere to the substratum. Regions of the lamellipod extending over nonadhesive surfaces retract within 5 minutes after the initial protrusion while regions which extend over adhesive surfaces are stabilized. In MTLn3 cells, ruffling is correlated with retraction of lamellipods rather than extension of lamellipods. The ruffles present on the upper surfaces of MTLn3 cells disappear transiently upon stimulation with EGF (Figure 20). After lamellipod extension has reached its maximum, then ruffling resumes. This is consistent with analyses of random fibroblast motility which also indicate that lamellipods which are not stabilized by attachment to the substratum are retracted via ruffles and then disappear(89,90). From this point of view, the ruffling that is observed upon expression of activated forms of rac (143) may reflect 1) stabilization of ruffles derived from randomly extended lamellipods by inhibition of the normal mechanism of lamellipod dissolution, 2) increased numbers of lamellipods which were unable to form stable contacts with the substratum resulting in increased numbers of retractions, 3) lamellipods which were generated in regions of the cell not in contact with the substratum or 4) increased number of retractions. Distinguishing between these different possibilities would aid in evaluating the actual mechanism by which rac functions. This is particularly relevant given the recent proposal that rac may activate LIM kinase, resulting in the inhibition of severing activity by cofilin (120,121).

It appears likely that stabilization of extended lamellipods occurs through formation of focal adhesions. Interference reflection microscopy of MTLn3 cells responding to EGF stimulation indicates the formation of focal contacts at times during which stabilization occurs (Figure 21). During the initial extension of the lamellipod, the lamellipod is near the substratum, but there is no indication of the extremely close contacts typical of focal contacts. This is consistent with the evidence cited above indicating that direct molecular interactions with the substratum are not necessary during the process of lamellipod extension. By IRM, small focal contacts are visible in the region of lamellipod extension around 5 minutes of stimulation with EGF, and they increase in size over the next 10 minutes. At the same time, many of the focal contacts present prior to EGF stimulation are remodeled: some become more diffuse and disappear while others located near the rear of polarized cells are dragged or left behind. These observations are consistent with observations reported for randomly locomoting fibroblasts (144-147). This concomitant generation of new contacts and destabilization of old ones likely provides the cell with a good way to set up the adhesive asymmetry that is necessary for contractility based motility(58,148).

By simultaneous talin and phosphotyrosine staining of cells at various times after EGF stimulation, it appears that new focal contacts have increased phosphotyrosine content compared to older focal contacts. Using talin as a marker for focal contacts, before EGF stimulation there are a number of mature focal contacts which are also identifiable by phosphotyrosine labeling (Figure 22). Five minutes following EGF stimulation, increased numbers of small, new focal contacts are present in the extended lamellipod (see also (33)). The larger mature focal contacts present at this time show less or no phosphotyrosine staining. This suggests that there is a differential effect of EGF stimulation on newly forming and preexisting focal contacts. It is possible that dephosphorylation of the older focal contacts destabilizes them while new focal contacts which are formed are not destabilized. This could weaken the preexisting interactions with the substrate, allowing easier detachment at the rear to facilitate movement, while

strengthening interactions at the front to stabilize the lamellipod. This, in conjunction with proteolytic cleavage of cytoskeletal linkages by molecules such as calpain (149,150) at the rear of the cell, would provide a mechanism for maintaining or enhancing cell polarization in the direction of lamellipod extension.

The key point suggested by this result is that both formation and dissolution of focal contacts may be stimulated by chemoattractants in order to facilitate cell polarization. Although growth factor stimulation has been shown to produce increases in focal contacts and tyrosine phosphorylation in a number of cell types, EGF stimulation leads to a general disruption of focal contacts in NR6 fibroblasts (78)and A431 cells(151,152). This correlates with a reduction in adhesion to the substratum for these cell types, as opposed to stimulation of adhesion of MTLn3 cells by EGF(101). The differences between various cell types may be reconciled by assuming that there are differences in the relative strengths of two competing processes - increases in new focal contacts due to lamellipod extension and dissolution of old focal contacts due to removal of phosphotyrosine. The relative strengths of these two processes could be dependent on the orientation of the projections that are generated. If cells do not generate lamellipods, or tend to produce ruffles that do not contact the substratum, then the number of new focal contacts may be relatively few. In that case, the dissolution of old focal contacts may predominate. In cells in which there is extensive production of flat lamellipods, large numbers of new focal contacts may be formed and the net effect is an increase in adhesion. A detailed analysis of the location of new focal contact formation in other cell types might aid in determining if this is correct. Alternatively, the effects on adhesion may reflect differences in relative strengths of intracellular signaling pathways. For example, high MAP kinase activity may result in extensive loss of focal contacts(78), perhaps through stimulation of a tyrosine phosphatase.

In conclusion, from the studies of MTLn3 cells, we propose the following series of events as occurring during chemotactic responses to EGF. Upon exposure to a gradient of EGF, activated EGF receptors near the edges of the cell stimulate a local increase in actin

polymerization sites. The polymerization of new actin filaments at these sites pushes the membrane out along the substratum, resulting in the extension of a lamellipod. Simultaneously, inhibition of ruffling occurs together with dephosphorylation of old focal contacts. As new focal contacts form in the region of lamellipod extension that is in contact with the substratum, the cell becomes reoriented towards the newly extended lamellipod, and contraction along stress fibers and within the cell body leads to detachment of the old contact sites and net movement of the cell into the extending lamellipod.

This process would be useful for movement of tumor cells through connective tissue in a number of ways. By extending lamellipods towards the source of chemoattractant, cells can be stimulated to leave the primary tumor and move out into connective tissue. Because the extending lamellipod does not require continuous contact with extracellular matrix, it can jump across small gaps in the matrix, or from one fiber to another. Finally, regions of the lamellipod that do contact new matrix sites become stabilized, enhancing the ability of the cell move into new regions. Visualization of tumor cell movement in situ will be the next stage in evaluating the process of tumor cell dispersal from the primary tumor in more detail. Availability of GFP-labeled cell models facilitate this, as recently shown for metastatic cells in vivo (Figure 23, (153)).

A number of intriguing questions remain to challenge our understanding of this process, however. First, what is the mechanism by which actin polymerization is restricted to the edge of the extending lamellipod? Why isn't actin polymerization stimulated along the entire upper surface? The EGF receptor appears to be uniformly distributed before EGF stimulation(Bailly et al., unpublished), so that presumably activation could occur along the entire upper surface of the cell, which clearly does not occur. Potentially there is an interaction with integrins which is necessary for establishing the site of actin polymerization but which then does not require further interaction with extracellular matrix once the activation is initiated. Second, what is the mechanism by which ruffling is suppressed? Is it simply a mechanical tension effect in which extension of the membrane at sites of lamellipod extension causes an increase in membrane

tension which then compresses the ruffles, or are there internal biochemical signals which are triggering more rapid retraction of the ruffles? It is clear that actin depolymerization is stimulated by EGF as well, as can be shown by measuring loss of filamentous actin in cells treated with cytochalasin D and then stimulated with EGF (34,37). Finally, how is dephosphorylation and destabilization of old focal contacts achieved at the time EGF causes new attachments? Does this utilize a MAP kinase/ERK pathway?

Although some broad questions regarding the method by which specific proteins contribute to lamellipod extension are likely to have similar answers for varied cell types, a true understanding of the complete process of lamellipod extension in different cell types is likely to require detailed experimentation in each type of cell. This becomes particularly important when deciding how to develop clinical applications of our basic science knowledge to diseases involving specific cell types. A challenge for the future will be to develop methods for easily determining which mechanism for lamellipod extension is operating in a particular cell type.

For example, our studies of MTLn3 cell motility have brought our understanding of the in vitro cell biology of mammary adenocarcinoma cells to a relatively advanced stage compared to our understanding of the general process of metastasis. The next phase in deepening our understanding of how in vitro cell biology relates to metastasis will require more sophisticated methods for dissecting the process of metastasis into its component steps. Once such methods are developed, we will be able to quantitate the abilities of cell lines with particular defects to reach a particular stage during metastasis (i.e., intravasation, extravasation, and growth in target organ), and compare those abilities with the defects measured in vitro. With a better understanding how a specific cell behavior contributes to the metastatic process, it may be possible to predict whether that behavior is the best target for developing new therapies.

REFERENCE LIST

1. S. Aznavoorian, A.N. Murphy, W.G. Stetler-Stevenson, L.A. Liotta, *Cancer* **71**, 1368 (1993).

2. G.L. Nicolson, *Biochemical Society Symposia* **63**, 231 (1998).

3. M.I. Cockett, *et al*, *Biochemical Society Symposia* **63**, 295 (1998).

4. E.C. Woodhouse, R.F. Chuaqui, L.A. Liotta, *Cancer* **80**, 1529 (1997).

5. A. Ahmad, I.R. Hart, *Critical Reviews in Oncology-Hematology* **26**, 163 (1997).

6. J. Rak, J. Filmus, R.S. Kerbel, *European Journal of Cancer* **32A**, 2438 (1996).

7. K. Engels, S.B. Fox, A.L. Harris, *EXS* **79**, 113 (1997).

8. T.J. de Vries, G.N. van Muijen, D.J. Ruiter, *Pathology, Research & Practice* **192**, 718 (1996).

9. J.T. Price, M.T. Bonovich, E.C. Kohn, *Critical Reviews in Biochemistry & Molecular Biology* **32**, 175 (1997).

10. K. Dhingra, G.N. Hortobagyi, *Seminars in Oncology* **23**, 436 (1996).

11. G.V. Scagliotti, P. Masiero, E. Pozzi, *Lung Cancer* **12 Suppl 1**, S13 (1995).

12. E.R. Sherwood, C. Lee, *World Journal of Urology* **13**, 290 (1995).

13. J.G. Klijn, *et al*, *Breast Canc.Res.Treat.* **29**, 73 (1994).

14. N.E. Hynes, D.F. Stern, *Biochimica et Biophysica Acta* **1198**, 165 (1994).

15. C.R. De Potter, A.M. Schelfhout, *Virchows Archiv* **426**, 107 (1995).

16. S.A. Chrysogelos, R.B. Dickson, *Breast Cancer Research & Treatment* **29**, 29 (1994).

17. N. Quenel, *et al*, *Breast Cancer Research & Treatment* **35**, 283 (1995).

18. S. Lewis, *et al*, *J.Clin.Path.* **43**, 385 (1990).

19. S. Nicholson, *et al*, *Br.J.Canc.* **63**, 146 (1991).

20. M. Toi, A. Osaki, H. Yamada, T. Toge, *Eur.J.Cancer* **27**, 977 (1991).

21. F. Battaglia, *et al*, *Eur.J.Canc.Clin.Onc.* **24**, 1685 (1988).

22. W. Wels, *et al*, *International Journal of Cancer* **60**, 137 (1995).

23. J. Baselga, *et al*, *Journal of Clinical Oncology* **14**, 737 (1996).

24. R. Repp, *et al*, *Journal of Hematotherapy* **4**, 415 (1995).

25. X. Han, N. Kasahara, Y.W. Kan, *Proc.Natl.Acad.Sci.USA* **92**, 9747 (1995).

26. D.R. Welch, A. Neri, G.L. Nicolson, *Inv.Met.* **3**, 65 (1983).

27. J.E. Segall, *et al*, *Clin.Exp.Met.* **14**, 61 (1996).

28. A.M. Kaufmann, *et al*, *Int.J.Oncol.* **4**, 1149 (1994).

29. R.B. Lichtner, *et al*, *J Biol.Chem.* **267**, 11872 (1992).

30. J. Condeelis, *Ann.Rev.Cell Biol.* **9**, 411 (1993).

31. S.H. Zigmond, *Curr.Opin.Cell Biol.* **8**, 66 (1996).

32. K. Barkalow, J.H. Hartwig, *Biochemical Society Transactions* **23**, 451 (1995).

33. M. Bailly, L. Yan, G.M. Whitesides, J.S. Condeelis, J.E. Segall, *Experimental Cell Research* **241**, 285 (1998).

34. A.Y. Chan, *et al*, *J.Cell Sci.* **111**, 199 (1998).

35. R.J. Eddy, J. Han, J.S. Condeelis, *J Cell Biol.* **139**, 1243 (1997).

36. K. Barkalow, W. Witke, D.J. Kwiatkowski, J.H. Hartwig, *J Cell Biol.* **134**, 389 (1996).

37. J.B. Wyckoff, *et al*, *Exp.Cell Res.* (1998)., in press

38. S. Kaufmann, J. Kas, W.H. Goldmann, E. Sackmann, G. Isenberg, *Febs Letters* **314**, 203 (1992).

39. B.T. Edmonds, *et al*, *J.Cell Sci.* **109**, 2705 (1996).

40. M.D. Welch, A.H. DePace, S. Verma, A. Iwamatsu, T.J. Mitchison, *J Cell Biol.* **138**, 375 (1997).

41. M.H. Symons, T.J. Mitchison, *J Cell Biol.* **114**, 503 (1991).

42. S. Okabe, N. Hirokawa, *J Cell Biol.* **109**, t (1989).

43. J.A. Ursitti, V.M. Fowler, *J Cell Sci.* **107**, 1633 (1994).

44. J.A. Ursitti, J.B. Wade, *Cell Motility.& the.Cytoskeleton* **25**, 30 (1993).

45. J.H. Hartwig, *J.Cell Biol.* **118**, 1421 (1992).

46. W. Kabsch, J. Vandekerckhove, *Annual.Review.of Biophysics.& Biomolecular.Structure.* **21**, 49 (1992).

47. T. Pollard, *J.Cell Biol.* **103**, 2747 (1986).

48. R.D. Mullins, J.A. Heuser, T.D. Pollard, *Proc.Natl.Acad.Sci.U.S.A* **95**, 6181 (1998).

49. L.M. Machesky, M. Way, *Nature* **394**, 125 (1998).

50. R. Niederman, P. Amrein, J. Hartwig, *J.Cell Biol.* **96**, 1400 (1983).

51. J. Hartwig, P. Shevlin, *J.Cell Biol.* **1037**, 1007 (1986).

52. J.V. Small, J.E. Celis, *Cytobiologie* **16**, 308 (1978).

53. J.V. Small, G. Isenberg, J.E. Celis, *Nature* **272**, 638 (1978).

54. J.V. Small, *Electron Microscopy.Reviews.* **1**, 155 (1988).

55. M.I. Ryder, R.N. Weinreb, R. Niederman, *Anatomical.Record.* **209**, 7 (1984).

56. D. Cox, J.A. Ridsdale, J. Condeelis, J. Hartwig, *J Cell Biol.* **128**, 819 (1995).

57. S. Rubino, J.V. Small, *Protoplasma* **136**, 63 (1987).

58. T.M. Svitkina, A.B. Verkhovsky, K.M. McQuade, G.G. Borisy, *J Cell Biol.* **139**, 397 (1997).

59. J.V. Small, *J Cell Biol.* **91**, t (1981).

60. J.V. Small, M. Herzog, K. Anderson, *J Cell Biol.* **129**, 1275 (1995).

61. H.L. Yin, J.H. Hartwig, *J.Cell Sci.Suppl.* **9**, 169 (1988).

62. M. Cano, D. Lauffenburger, S. Zigmond, *J.Cell Biol.* **115**, 677 (1991).

63. J.L. Podolski, T.L. Steck, *J Biol.Chem.* **265**, 1312 (1990).

64. R.D. Mullins, J.A. Heuser, T.D. Pollard, *Proceedings.of the.National.Academy.of Sciences.of the.United.States.of America.* **95**, 6181 (1998).

65. J.J. Wolosewick, J. Condeelis, *J.Cell Biochem.* **30**, 227 (1986).

66. J.H. Hartwig, J. Tyler, T.P. Stossel, *J Cell Biol.* **87**, t (1980).

67. C.C. Cunningham, *et al, Science* **255**, 325 (1992).

68. L.W. Janson, K. Ragsdale, K. Luby-Phelps, *Biophysical.Journal* **71**, 1228 (1996).

69. M.D. Welch, A. Iwamatsu, T.J. Mitchison, *Nature* **385**, 265 (1997).

70. R. Nagaoka, H. Abe, T. Obinata, *Cell Motility & the Cytoskeleton* **35**, 200 (1996).

71. S. Djafarzadeh, V. Niggli, *Experimental Cell Research* **236**, 427 (1997).

72. P.G. Heyworth, J.M. Robinson, J. Ding, B.A. Ellis, J.A. Badwey, *Histochemistry & Cell Biology* **108**, 221 (1997).

73. H. Aizawa, Y. Fukui, I. Yahara, *J Cell Sci.* **110**, 2333 (1997).

74. A. Moon, D.G. Drubin, *Mol.Biol.Cell* **6**, 1423 (1995).

75. M.D. Welch, J. Rosenblatt, J. Skoble, D.A. Portnoy, T.J. Mitchison, *Science* **281**, 105 (1998).

76. C. Albiges-Rizo, P. Frachet, M.R. Block, *J Cell Sci.* **108**, 3317 (1995).

77. R.B. Lichtner, P.N. Belloni, G.L. Nicolson, *Experimental Cell Biology* **57**, 146 (1989).

78. H. Xie, *et al*, *J Cell Sci.* **111**, 615 (1998).

79. A. Neri, D. Welch, T. Kawaguchi, G.L. Nicolson, *J.Natl.Cancer Inst.* **68**, 507 (1982).

80. A.M. Kaufmann, R.B. Lichtner, V. Schirrmacher, K. Khazaie, *Oncogene* **13**, 2349 (1996).

81. C.R. De Potter, A.M. Schelfhout, *Virchows Archiv* **426**, 107 (1995).

82. D.L. Taylor, J.S. Condeelis, *International Review of Cytology* **56**, 57 (1979).

83. M. Demma, V. Warren, R. Hock, S. Dharmawardhane, J. Condeelis, *J.Biol.Chem.* **265**, 2286 (1990).

84. R.A. Edwards, J. Bryan, *Cell Motility & the Cytoskeleton* **32**, 1 (1995).

85. S.B. Kater, V. Rehder, *Current Opinion in Neurobiology* **5**, 68 (1995).

86. D. Wessels, H. Vawter-Hugart, J. Murray, D.R. Soll, *Cell Motility & the Cytoskeleton* **27**, 1 (1994).

87. L.P. Cramer, M. Siebert, T.J. Mitchison, *J Cell Biol.* **136**, 1287 (1997).

88. P. Matsudaira, *Sem.Cell Biol.* **5**, 165 (1994).

89. M. Abercrombie, J.E. Heaysman, S.M. Pegrum, *Experimental Cell Research* **60**, 437 (1970).

90. J.P. Heath, B.F. Holifield, *Symposia of the Society for Experimental Biology* **47**, 35 (1993).

91. J.E. Segall, *Proc.Natl.Acad.Sci.U.S.A.* **90**, 8332 (1993).

92. J.E. Segall, G. Gerisch, *Curr.Opin.Cell Biol.* **1**, 44 (1989).

93. C. Dong, S. Aznavoorian, L.A. Liotta, *Microvascular Research* **47**, 55 (1994).

94. H.C. Chen, *et al*, *J Biol.Chem.* **270**, 16995 (1995).

95. A.A. Noegel, J.E. Luna, *Experientia* **51**, 1135 (1995).

96. P.J. Van Haastert, *Experientia* **51**, 1144 (1995).

97. M.Y. Chen, R.H. Insall, P.N. Devreotes, *Trends in Genetics* **12**, 52 (1996).

98. J. Chant, *Curr.Op.Cell Biol.* **8**, 557 (1996).

99. E. Leberer, D.Y. Thomas, M. Whiteway, *Current Opinion in Genetics & Development* **7**, 59 (1997).

100. J.B. Welsh, G.N. Gill, M.G. Rosenfeld, A. Wells, *J Cell Biol.* **114**, 533 (1991).

101. R.B. Lichtner, M. Wiedemuth, C. Noeske-Jungblut, V. Schirrmacher, *Clin.Exp.Met.* **11**, 113 (1993).

102. M. Chinkers, J.A. McKanna, S. Cohen, *J.Cell Biol.* **83**, 260 (1979).

103. M.D. Welch, A. Mallavarapu, J. Rosenblatt, T.J. Mitchison, *Curr.Op.Cell Biol.* **9**, 54 (1997).

104. K. Barkalow, J.H. Hartwig, *Biochemical Society Transactions* **23**, 451 (1995).

105. K.R. Ayscough, *Curr.Opin.Cell Biol.* **10**, 102 (1998).

106. K. Burridge, M. Chrzanowska-Wodnicka, *Annual Review of Cell & Developmental Biology* **12** , 463 (1996).

107. J.A. DePasquale, C.S. Izzard, *J Cell Biol.* **113**, 1351 (1991).

108. K.M. Yamada, B. Geiger, *Curr.Op.Cell Biol.* **9**, 76 (1997).

109. C.D. Nobes, A. Hall, *Cell* **81**, 53 (1995).

110. G.H. Nuckolls, L.H. Romer, K. Burridge, *J Cell Sci.* **102**, 753 (1992).

111. L.M. Machesky, S.J. Atkinson, C. Ampe, J. Vandekerckhove, T.D. Pollard, *J Cell Biol.* **127**, 107 (1994).

112. L.M. Machesky, *et al, Biochemical Journal* **328**, 105 (1997).

113. R.D. Mullins, J.F. Kelleher, J. Xu, T.D. Pollard, *Mol.Biol.Cell* **9**, 841 (1998).

114. L.M. Machesky, *Curr.Biol.* **7**, R164 (1997).

115. P. Cossart, *Curr.Op.Cell Biol.* **7**, 94 (1995).

116. L.A. Lopez, M.P. Sheetz, *Journal of Biological.Chemistry.* **270**, 12511 (1995).

117. J.A. Theriot, *J Cell Biol.* **136**, 1165 (1997).

118. M.F. Carlier, *Curr.Op.Cell Biol.* **10**, 45 (1998).

119. H. Aizawa, K. Sutoh, I. Yahara, *J Cell Biol.* **132**, 335 (1996).

120. N. Yang, *et al, Nature* **393**, 809 (1998).

121. S. Arber, *et al, Nature* **393**, 805 (1998).

122. N.A. Maun, D.W. Speicher, M.J. DiNubile, F.S. Southwick, *Biochemistry* **#19;35**, 3518 (1996).

123. V.M. Fowler, *Curr.Op.Cell Biol.* **8**, 86 (1996).

124. P.A. Kuhlman, C.A. Hughes, V. Bennett, V.M. Fowler, *J Biol.Chem.* **271**, 7986 (1996).

125. M. Tardif, *et al*, *J Biol.Chem.* **270**, 28075 (1995).

126. D.A. Schafer, P.B. Jennings, J.A. Cooper, *J Cell Biol.* **135**, 169 (1996).

127. A. McGough, W. Chiu, M. Way, *Biophysical Journal* **74**, 764 (1998).

128. W. Witke, *et al*, *Cell* **81**, 41 (1995).

129. P. Chen, J.E. Murphy-Ullrich, A. Wells, *J Cell Biol.* **134**, 689 (1996).

130. A. Arcaro, *J Biol.Chem.* **273**, 805 (1998).

131. J.S. Wang, J.P. Coburn, A.I. Tauber, K.S. Zaner, *Mol.Biol.Cell* **8**, 121 (1997).

132. M. Schleicher, *et al*, *Febs Letters* **369**, 38 (1995).

133. D.A. Schafer, J.A. Cooper, *Annual Review of Cell & Developmental Biology* **11**, 497 (1995).

134. M.F. Carlier, D. Pantaloni, *Journal of Molecular Biology* **269**, 459 (1997).

135. M.J. DiNubile, S. Huang, *Cell Motility & the Cytoskeleton* **37**, 211 (1997).

136. E. Korenbaum, *et al*, *Biochemistry* **37**, 9274 (1998).

137. M.F. Carlier, D. Pantaloni, *Sem.Cell Biol.* **5**, 183 (1994).

138. L.A. Flanagan, *et al*, *Biophysical Journal* **73**, 1440 (1997).

139. K.M. Lin, E. Wenegieme, P.J. Lu, C.S. Chen, H.L. Yin, *J Biol.Chem.* **272**, 20443 (1997).

140. A. Mogilner, G. Oster, *Biophysical Journal* **71**, 3030 (1996).

141. L.P. Cramer, T.J. Mitchison, *J Cell Biol.* **131**, 179 (1995).

142. C.H. Lin, E.M. Espreafico, M.S. Mooseker, P. Forscher, *Neuron* **16**, 769 (1996).

143. N. Tapon, A. Hall, *Curr.Op.Cell Biol.* **9**, 86 (1997).

144. C.S. Izzard, *Cell Motility & the Cytoskeleton* **10**, 137 (1988).

145. C.S. Izzard, L.R. Lochner, *J Cell Sci.* **21**, 129 (1976).

146. C.S. Izzard, L.R. Lochner, *J Cell Sci.* **42**, 81 (1980).

147. S.P. Palecek, C.E. Schmidt, D.A. Lauffenburger, A.F. Horwitz, *J Cell Sci.* **109**, 941 (1996).

148. D.A. Lauffenburger, A.F. Horwitz, *Cell* **84**, 359 (1996).

149. S.P. Palacek, A. Huttenlocher, A.F. Horwitz, D.A. Lauffenburger, *J.Cell Sci.* **111**, 929 (1998).

150. A. Huttenlocher, *et al*, *J Biol.Chem.* **272**, 32719 (1997).

151. M. Rieber, F. Gil, M.S. Rieber, C. Urbina, *International Journal of Cancer* **37**, 411 (1986).

152. E. Genersch, *et al*, *International Journal of Cancer* **75**, 205 (1998).

153. K.L. Farina, *et al*, *Canc.Res.* **58**, 2528 (1998).

BIBLIOGRAPHY OF ALL PUBLICATIONS AND MEETING ABSTRACTS

Publications

1. Segall, J.E., Tyerech, S., Boselli, L., W., Masseling, S., Chan, A., Helft, J, Jones, J. and J. Condeelis. (1996) EGF stimulates lamellipod extension and chemotaxis in metastatic mammary adenocarcinoma cells by an actin-dependent mechanism. *Clin. Exp. Met.* 14:61-72.
2. Edmonds, B.T., Wyckoff, J., Yeung, Y.-G., Wang, Y., Stanley, E.R., Jones, J., Segall, J.E., and J. Condeelis. (1996) Elongation factor-1alpha is an overexpressed actin binding protein in metastatic rat mammary adenocarcinoma. J. Cell Science 109:2705-2714.
3. Cammer, M., Wyckoff, J. and J.E. Segall (1997) Computer-assisted analysis of single cell motility. In: *Basic Cell Culture Protocols* (eds. J.M. Walker and J.W. Pollard), Methods in Molecular Biology, 75:459-470.
4. Chan, A., Raft, S., Bailly, M., Wyckoff, J., Segall, J. and Condeelis, J. (1998) EGF stimulates an increase in actin nucleation and filament number at the leading edge of the lamellipod in mammary adenocarcinoma cells. J. Cell Sci. 111:199-211.
5. Bailly, M., Yan, L., Whitesides, G.M., Condeelis, J.S., and J.E. Segall (1998) Interactions between protrusion and adhesion during chemotaxis of mammalian carcinoma cells. Exp. Cell Res. 241:285-299.
6. Farina, K.L., Wyckoff, J.B., Rivera, J., Lee, H., Segall, J.E., Condeelis, J.S., and J. G. Jones (1998) Cell motility of tumor cells visualized in living intact primary tumors using green fluorescent protein. Cancer Res. 58:2528-2532.
7. Wyckoff, J.B., Insel, L., Khazaie, K., Lichtner, R.B., Condeelis, J.S. and J.E. Segall (1998) Suppression of ruffling by the EGF receptor in chemotactic cells. Exp. Cell Res.242:100-109.
8. Zigmond, S.H., Foxman, E.F. and J.E. Segall (in press) Chemotaxis Assays for Eukaryotic Cells. In: Current Protocols in Cell Biology. (J. S. Bonifacina et al., eds) New York, John Wiley & Sons.
9. Bailly, M., Condeelis, J. and Segall, J.E. (in press) Chemoattractant-stimulated lamellipod extension. Microscopy Research and Technique.
10. Segall, J. E. (in press) Chemotaxis gets CRACking. Current Biology
11. Pestell, R. G., Albanese, C., Reutens, A.T., Lee, R.J., Segall, J.E., and A. Arnold. The cyclins and cyclin dependent kinase inhibitors in hormonal regulation of proliferation and differentiation. Endocrine Reviews.
12. Bailly, M., Macaluso, F., Cammer, M., Chan, A., Segall, J.E., and J. S. Condeelis. (submitted) Relationships between Arp2/3 complex and the barbed ends of actin filaments at the leading edge of carcinoma cells after EGF stimulation.

Meeting Abstracts

1. Bailly, M., Condeelis, J., and J. E. Segall (1996) Dynamics of lamellipod extension and focal adhesion assembly following EGF stimulation of metastatic mammary adenocarcinoma cells. Keystone Symposium on Cell Migration.
2. Segall, J.E., Bailly, M., Chan, A., Edmonds, B., Wyckoff, J., Jones, J., and J. Condeelis. (1997) Molecular Analysis of Chemotaxis in Breast Cancer Cells. Department of Defense Era of Hope, p. 675.
3. Chan, A. Bailly, M., Wyckoff, J., Segall, J. and J. Condeelis (1997) EGF stimulates an increase in actin nucleation and filament number at the tip of the lamellipod in mammary adenocarcinoma cells. ASCB Annual Meeting. Mol. Biol. Cell 8S: p. 257a

4. Segall, J.E., Insel, L., Khashayarsha, K., Lichtner, R.B., Condeelis, J.S., and Wyckoff, J.B. (1997) Suppression of Ruffling by EGF in chemotactic cells. . ASCB Annual Meeting. Mol. Biol. Cell 8S: p. 265a.
5. Farina, K.L., Wyckoff, J.B., Rivera, J., Lee, H., Segall, J.E., Condeelis, J.S., and J. G. Jones (1998) Cell motility of tumor cells visualized in living intact primary tumors using green fluorescent protein. Keystone Symposium on Motility and Metastasis.
6. Bailly, M., Chan, A., Segall, J.E. and J. Condeelis. (1998) Ultrastructural Definition of the polymerization zone induced at the leading edge of metastatic carcinoma cells after EGF stimulation. Keystone Symposium on Motility and Metastasis.

PERSONNEL RECEIVING PAY FROM THIS EFFORT

1. F. Abbate
2. M. Bailly
3. J. Condeelis
4. K. Gohari
5. E. Horowitz
6. J. Segall
7. J. Wykoff
8. Y. Yu
9. N. Zolta

FIGURE LEGENDS

Figure 1: Arp2/3 complex colocalizes with F-actin at the leading edge of cells after stimulation. Cells were stimulated with EGF for 3 min, fixed, permeabilized and immunostained for Arp2/3 complex using anti-Arp3 or anti-p21 antibodies, and for actin using anti-actin antibodies. Fluorescence measurements were done as described in Material and Methods. **A.** Both Arp3 and p21 localize in the actin rich zone at the extreme periphery of the cells (matching arrowheads). Panels **1**, **3**, actin; panel **2**, Arp3; panel **4**, p21. Box indicates the region at the leading edge where all further analyses were done, including electron microscopy. Bar, 10 um. **B**. Quantitation of immunofluorescence showing precise colocalization of Arp2/3 and actin within 1.5 um at the leading edge. Boxed area in panel **1** above shows a portion of the circumferential zone in the lamellipod where the measurements were done. The fluorescence intensity graphed is the mean of the entire cell perimeter for 1 pixel wide steps (see Material and Methods). (gray diamonds), actin; (circles), Arp3; (squares), p21. Both Arp2/3 (Arp3 and p21) and actin concentrations peak within 0.5 um of the leading edge. The increase in fluorescence intensity that is observed further back from the membrane is due to interference from stress fibers for the actin and dense particles for Arp3 and p21, and emphasizes the need to use electron microscopy in this analysis.

Figure 2: Kinetics of appearance of nucleation sites at the leading edge after EGF stimulation. Cells were stimulated with EGF and permeabilized for 1 min in the presence of 0.45 uM rhodamine-actin. They were then fixed and pictures were taken at constant settings. Nucleation activity was measured as rhodamine fluorescence incorporation (34). Fluorescence intensity was measured as the mean pixel intensity within 1.1 um of the circumferential membrane at the leading edge of the cells (see boxed area in Figure 1A). Results are the mean of 3 different experiments, with a total of 10-20 cells measured in each experiment.

Figure 3: Arp2/3 complex colocalizes with EGF-stimulated nucleation activity at the leading edge of the cells. Cells were stimulated with EGF and permeabilized in the presence of 0.45 uM rhodamine-labeled actin for 1 min, and then fixed and stained for Arp2/3 localization as described in Material and Methods. In unstimulated cells (EGF0), Arp3 is enriched in the peripheral submembraneous compartment and, in conjunction with nucleation activity, in ruffling areas (asterisk). One minute after EGF stimulation (EGF1), Arp3 is recruited homogeneously to the extreme edge of the cells in conjunction with the newly created nucleation sites (arrowheads), as well as in particulate bodies (arrows). After 3 minutes (EGF3), nucleation activity remains confined to the very submembraneous compartment and the tips of the stress fibers (presumably focal contacts), while the Arp3 distribution is restricted to the leading edge where it tends to extend beyond the nucleation site location, further inside the cell (concave arrowheads). Bar, 20 um.

Figure 4: Negative staining of MTLn3 cells permeabilized in presence of biotin-labeled actin. Cells were stimulated with EGF and permeabilized for 1 min in presence of 0.45 uM biotin-labeled actin. They were then fixed, immunolabeled with anti-biotin antibodies coupled to 5 nm gold particles, and negatively stained with 1% phosphotungstic acid. Image shows a low magnification of a typical leading edge 1 min after EGF stimulation, where a dense actin network is visible at the extreme edge (facing arrows). The line shows where the membrane position was set for morphometric analysis. Bar, 1 um.

Figure 5: Ultrastructural localization of the nucleation sites in negatively stained leading edges. Cells were stimulated with EGF and permeabilized for 1 min in presence of 0.45 uM biotin-labeled actin. They were then fixed, immunolabeled with anti-biotin antibodies coupled to 5 nm gold particles, and negatively stained with 1% phosphotungstic acid. **A**, unstimulated cell edge not organized as a typical lamellipod. Note the loose network and occasional bundling of the filaments, as well as very low biotin-labeled actin incorporation. **B**, leading edge of a

lamellipod in an unstimulated cell, organized as a network of dense filaments. Note the filaments growing radially from the edge (arrows), and the biotin-labeled actin incorporation (arrowheads). **C**, leading edge of a cell 1 min after stimulation with EGF. The network of actin filament is denser and the biotin-labeled actin incorporation is abundant. **D**, Schematic description of the way the distribution of gold particles was analyzed at the leading edge for morphometric analysis: boxes of 1 x 0.1 um^2 are shown here as an example. All the analyses were done with 2 x 0.1 um^2 boxes (see Material and Methods).**mb**, membrane position (see figure 4). A-D, bar 0.3 um.

Figure 6: Morphometric analysis of the distribution of the nucleation sites and filament density at the leading edge. **A**, quantitation of nucleation activity at the leading edge was done on negatively stained samples by analyzing the distribution of the gold particles reflecting biotin-labeled actin incorporation, using a macro designed for NIH Image (see Materials and Methods). The particles were counted in 2 x 0.1 um^2 contiguous boxes starting outside the cell and going back about 2 microns inside the cell (Figure 5D). (squares), unstimulated cells, non lamellipod-like edges (see Figure 5A); (open circles), leading edges in unstimulated cells (see Figure 5B); (triangles), EGF 30 sec; (diamonds), EGF 1 min (see Figure 5C); (stars), EGF 3 min; (closed circles), EGF 5 min. **B**, quantitation of filament density was done on the same set of negatively stained samples as in **A**, with a slight adaptation of the method: 5 lines were drawn perpendicularly to the leading edge, and total filaments that crossed the 5 lines were analyzed using the same macro as in A (see Material and Methods). Legend same as in A, except that (squares) unstimulated cells in regions with no typical leading edge are not shown.

Figure 7: 3-D organization of the cytoskeleton at the leading edge. Cells were stimulated with EGF, permeabilized in the presence of 0.45 uM biotin-actin, and then fixed and processed for immunostaining with 5 nm gold conjugated anti-biotin antibodies. After post-fixation, samples were treated for rotary shadow as described in Material and Methods. **A**. General architecture of

the cytoskeleton at the leading edge of the cells 1 min after stimulation with EGF. Note the high density network at the extreme edge (brackets), and the decrease in filament density away from the edge. **B**, bundles of actin filaments at the periphery of a resting cell (arrow). **C**, leading edge of a lamellipod in a cell 1 min after EGF stimulation. **D**, higher magnification of C. **E**, higher magnification of D (stereo view). Note the gold particles decorating the filaments at the extreme edge of the lamellipod (arrows). **F**, Different types of branching observed at the leading edge: branching (arrow) on a filament growing radially from the edge that had incorporated exogenous biotin-actin (panel 1); ~70° (Arp2/3-type) branching on unlabeled filaments inside the network (panel 2, arrow); T-branching inside the network at the leading edge (panels 3, 4 and 5, arrowheads); Y-branching with small angles inside the network (panel 2 concave arrowhead). **G**, filament length measurement at the leading edge. Most of the filaments measured were growing radially from the edge (panel 1), some were measured inside the network (panel 2). Filaments were traced to their origin as shown and the length was measured using NIH Image. Arrowheads mark the 2 ends of the filaments. A-D, bar 0.5 um. E, bar, 0.2 um. F, G, bar 0.05 um.

Figure 8. Filament length distribution within a 1 um zone at the leading edge. Filament length was measured on samples processed for FDS using NIH Image (see Figure 7G, and Material and Methods). **A**, cell edges not organized as typical leading edges in resting cells (see Figure 7B); mean filament length: 314±8 nm, n=467. **B**, leading edges in resting cells; mean filament length 208±8 nm, n=198. **C**, leading edges in cell stimulated with EGF for 1 min (see Figure 7C); mean filament length: 179±4, n=628. **D**, leading edges in cells stimulated with EGF for 3 min; mean filament length: 189±5, n=334.

Figure 9: Arp3 and p21 are recruited to the leading edge after stimulation. Cells were permeabilized in presence of 0.45 uM biotin-actin, and then fixed and processed for immunostaining with 5 nm gold conjugated anti-biotin antibodies and rabbit anti-Arp3 or rabbit anti-p21 antibodies followed by 10 nm gold-conjugated anti-rabbit antibodies. Samples were

then negatively stained with 1% phosphotungstic acid and the distribution of the particles was analyzed in NIH Image (see Figure 5D and Material and Methods). Both 5 nm and 10 nm gold particle distributions were recorded on the same samples, with the same reference towards the membrane. EGF0, unstimulated cells; EGF1, cells stimulated for 1 min with EGF; EGF3, cells stimulated for 3 min with EGF. The vertical bar marks the position of the membrane.

Figure 10: Colocalization of Arp3 and gelsolin-capped actin barbed ends at the leading edge. Arp3 distribution is not offset from that of the nucleation sites when the EGF-generated free barbed ends are prevented from polymerizing using gelsolin-actin complexes (b-GA2). Cells were permeabilized in presence of 100 nM biotin-labeled gelsolin-actin complexes GA2, and then fixed and processed for immunostaining with 5 nm gold conjugated anti-biotin antibodies and rabbit anti-Arp3 antibodies followed by 10 nm gold-conjugated anti rabbit antibodies. Samples were then negatively stained with 1% phosphotungstic acid. (squares), unstimulated cells; (circles), cells stimulated with EGF for 1 min; (triangles), cells stimulated with EGF for 3 min. The vertical bar marks the position of the membrane.

Figure 11: Western blot of talin protein. In clone 10, growth in the absence of tetracycline results in a 50% reduction in the amount of talin protein. A stable hygromycin-resistant clone (clone 10) derived from MTLn3 cells transfected with the talin antisense vector was grown in the presence of tetracycline (to suppress antisense transcription) or the absence of tetracycline (to allow antisense mRNA transcription). Samples were collected and equal amount of total protein applied to the gel in varying dilutions from 100% to 12.5%.

Figure 12: Focal contact production is reduced in the talin antisense transfectant. Parental MTLn3 and clone 10 cells were grown in the presence or absence of tetracycline. Cells were stimulated with EGF and fixed 3 minutes after stimulation, followed by staining for talin (left image of each pair) or F-actin (right image of each pair). MTLn3 cells and clone 10 cells grown

in the presence of tetracycline show clear focal contacts (arrows). Clone 10 cells grown in the absence of tetracycline (to induce expression of the talin antisense mRNA), show reduced numbers and sizes of focal contacts (bottom row).

Figure 13:EGF-induced lamellipod extension may not be altered in Clone 10 cells. Cells were stimulated with EGF between frames 3 and 4, and lamellipod extension was measured as a function of time after stimulation using total area as a marker.

Figure 14: Model of generation of nucleation sites at the leading edge after stimulation: cooperation of Arp2/3 complex and a cofilin-like severing activity. Numbers above arrows show the rate constants for each reaction (events/sec), calculated from the molar on-rate constants presented in Mullins et al (116) and assuming a G-actin concentration of 1 uM. Longer arrows show preferred direction for the reactions. The rate constant of assembly of actin monomers into a dimer virtually precludes spontaneous generation of actin dimers in vivo (dotted line). Similarly, the formation of a complex between Arp2/3 and one actin monomer, as well as addition of a second actin monomer to this complex to create a nucleus is extremely unlikely . We propose that severing of preexisting filaments by cofilin generates oligomers (n designates 2 or more subunits), that are then captured and stabilized by capping of pointed ends by the Arp2/3 complex to efficiently generate nucleation sites for actin polymerization.

Figure 15: MTLn3 cells display amoeboid chemotaxis. (A) An MTLn3 cell oriented towards a pipet filled with a solution of 50 uM EGF (time in the top left corner). The cell crawled towards the pipet and changed direction when the pipet was moved (arrow marks the moving pipet on image 16:31:04); bar, 20 um. (B) Difference images showing lamellipod extension at the front of the cell (light gray) and retraction at the rear (medium gray). Time is indicated as minutes after initial positioning of the pipet. The cell path over the course of the experiments is

shown as the position of the centroid of the cell once every minute on the top left image. From (33).

Figure 16: Lamellipod extension occurs in response to uniform increases in EGF concentration. Cells were imaged before (A) and 2.5 min after stimulation with 5 nM EGF. Ruffles are indicated by arrows and areas of lamellipod extension are indicated by arrowheads. Bar, 20 um. From (27).

Figure 17: EGF stimulates protrusive activity in cells in suspension. MTLn3 cells were stimulated in suspension with EGF, fixed 0, 2 and 5 minutes after stimulation, permeabilized and stained with rhodamine-labeled phalloidin. They were imaged with a confocal microscope and 3 D reconstructions formed from z series of representative cells after stimulation in suspension. Axis scale intervals, 10 um. From (33).

Figure 18: Filament growth at the leading edge of stimulated cells. Cells were stimulated for 1 min with EGF, permeabilized in presence of 0.45uM biotin-labeled actin for 1 min and fixed in 0.5% glutaraldehyde. They were then processed for immunogold labeling (5 nm gold coated antibodies) followed by quick freezing and rotary shadowing (1.3 nm tantalum/tungsten, 2.5 nm carbon coating). A, Stereo view of the cytoskeleton at the leading edge. B, Enlarged area from A, showing incorporation of biotin labeled actin in the filaments, as revealed by the gold particles distribution. Small arrows, individual 5 nm gold particles along actin filaments; large arrow, cluster of numerous gold particles of filaments growing perpendicularly to the surface; arrowheads, striations on the filaments showing individual actin monomers.

Figure 19: MTLn3 cells extend lamellipods over a nonadhesive substratum. MTLn3 cells were plated on gold-coated glass coverslips which were patterned with hexadecanthiol and EGF6-thiol to generate 10 um lanes of adhesive substratum. The cells were stimulated with 5

Figure 1

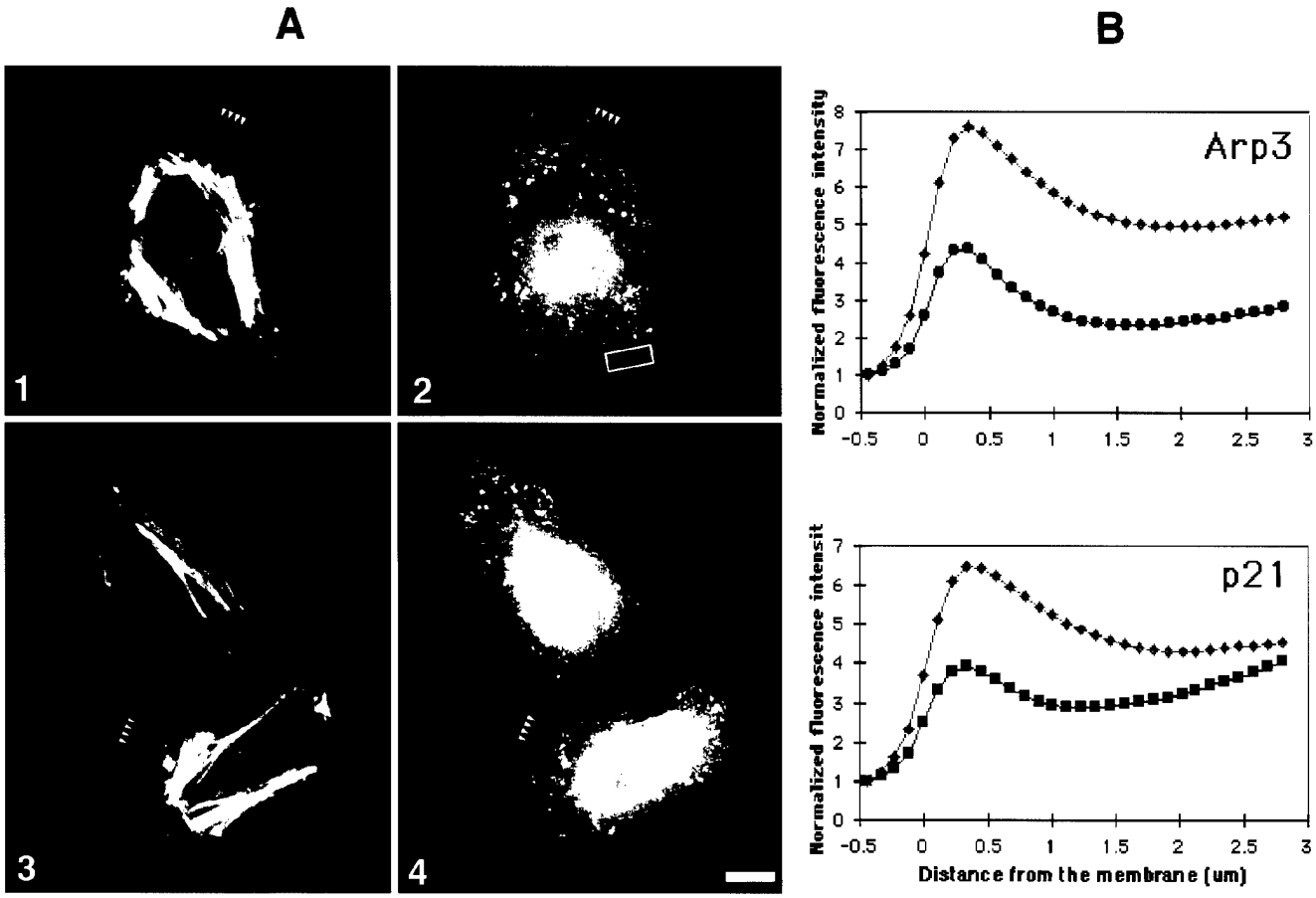

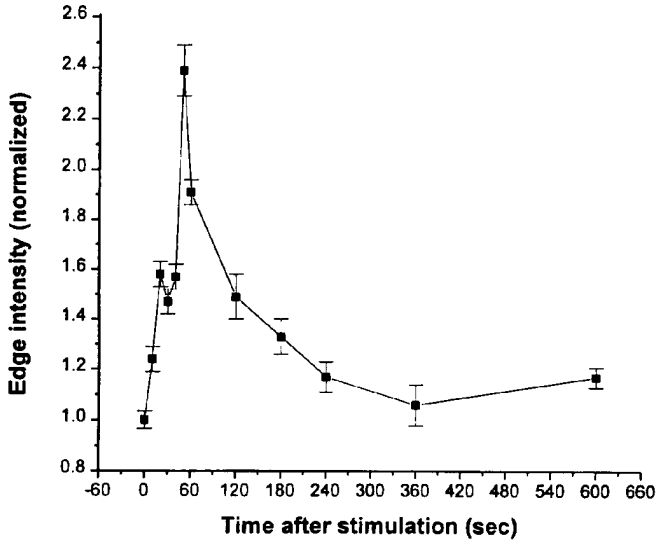

Figure 2

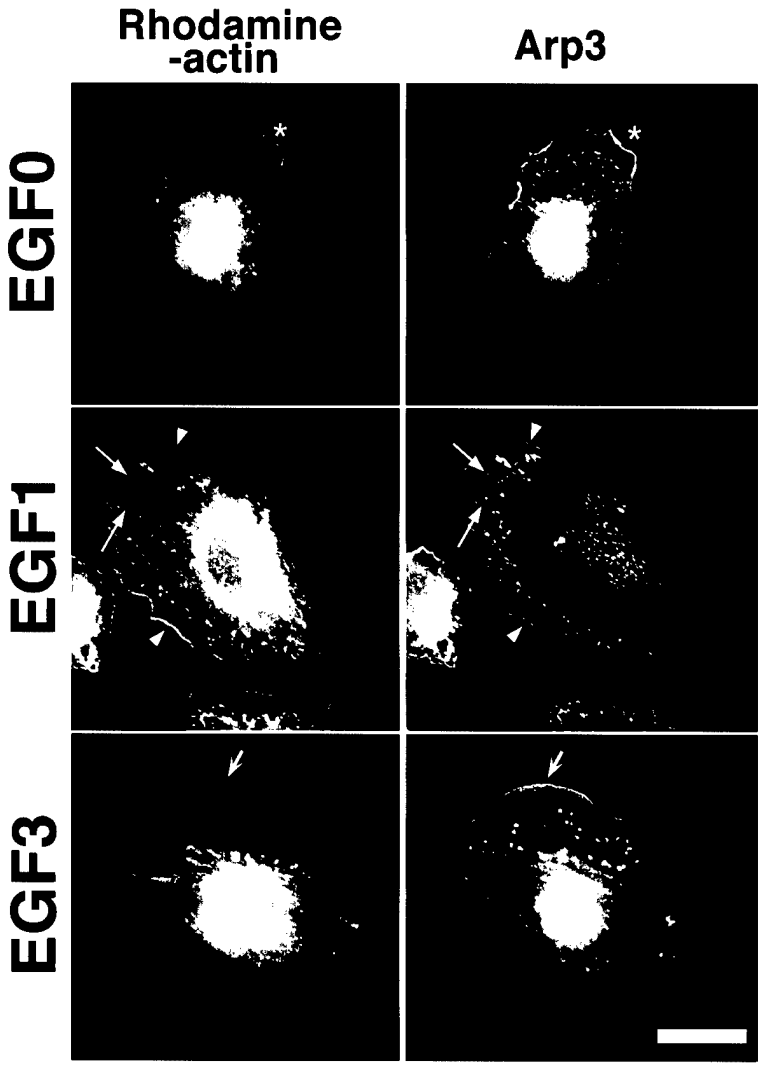

Figure 3

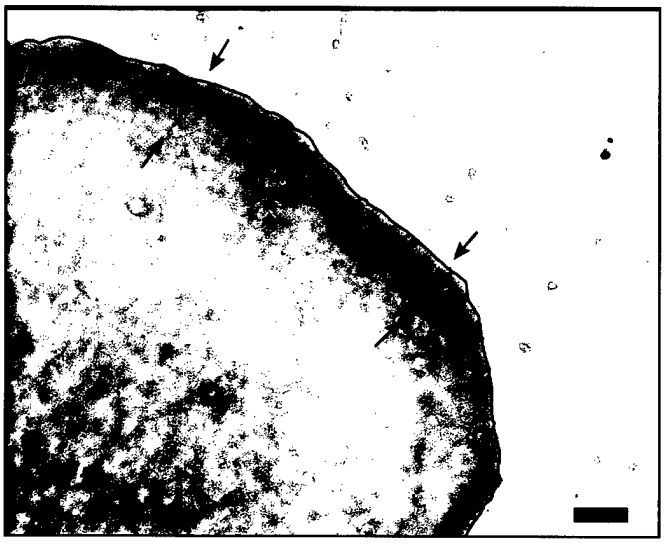

Figure 4

Figure 5

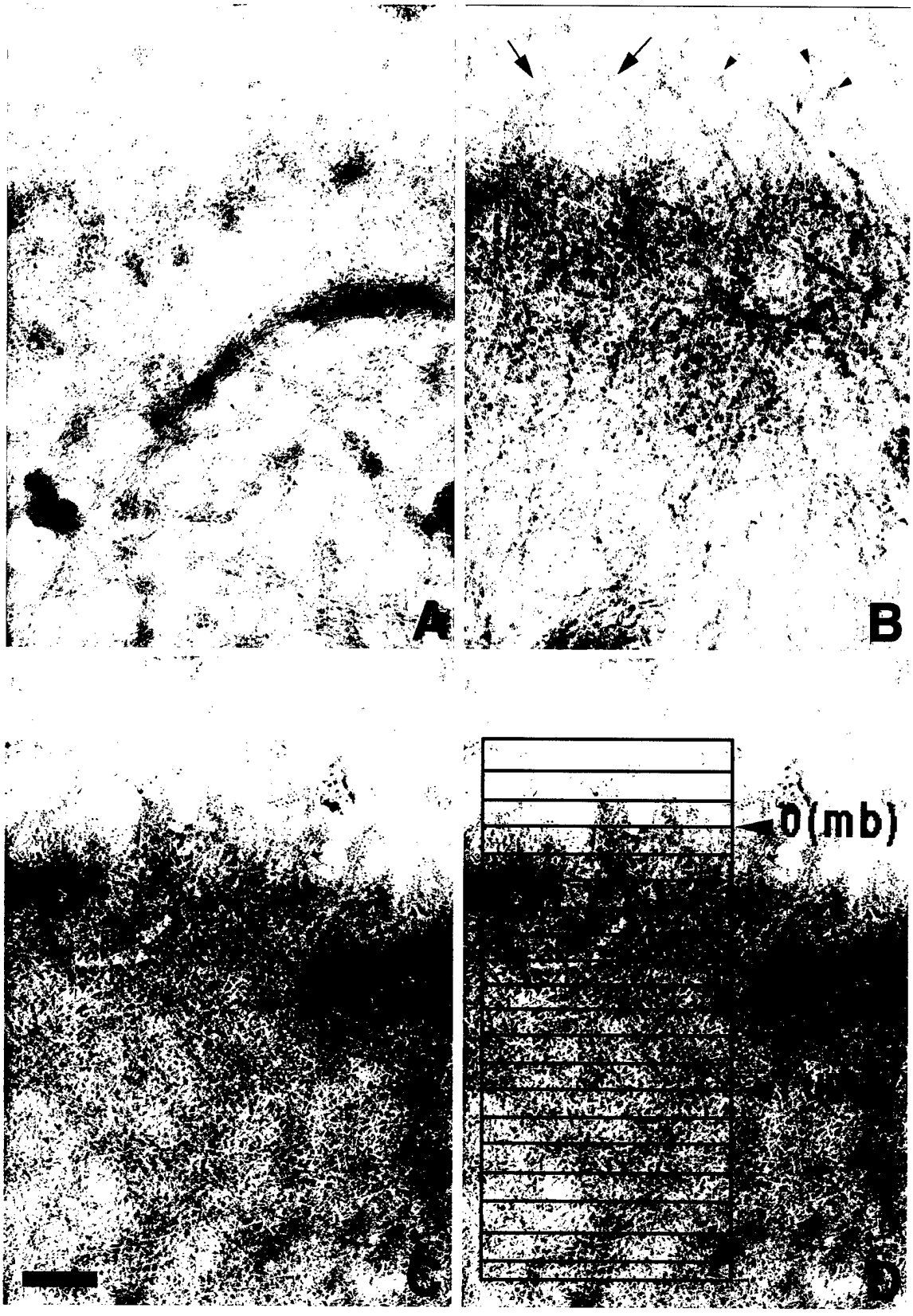

Figure 6

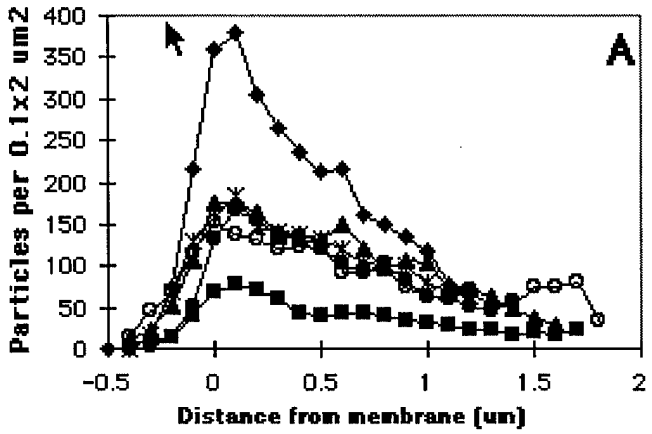
A
Particles per 0.1x2 um2
400
350
300
250
200
150
100
50
0
-0.5
0
0.5
1
1.5
2
Distance from membrane (um)

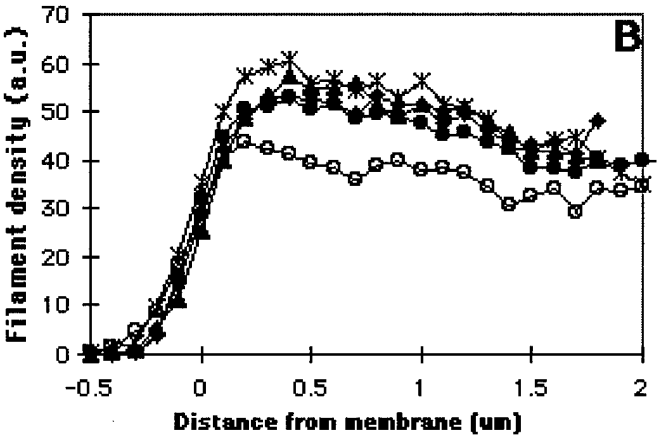
B
Filament density (a.u.)
70
60
50
40
30
20
10
0
-0.5
0
0.5
1
1.5
2
Distance from membrane (um)

Figure 7

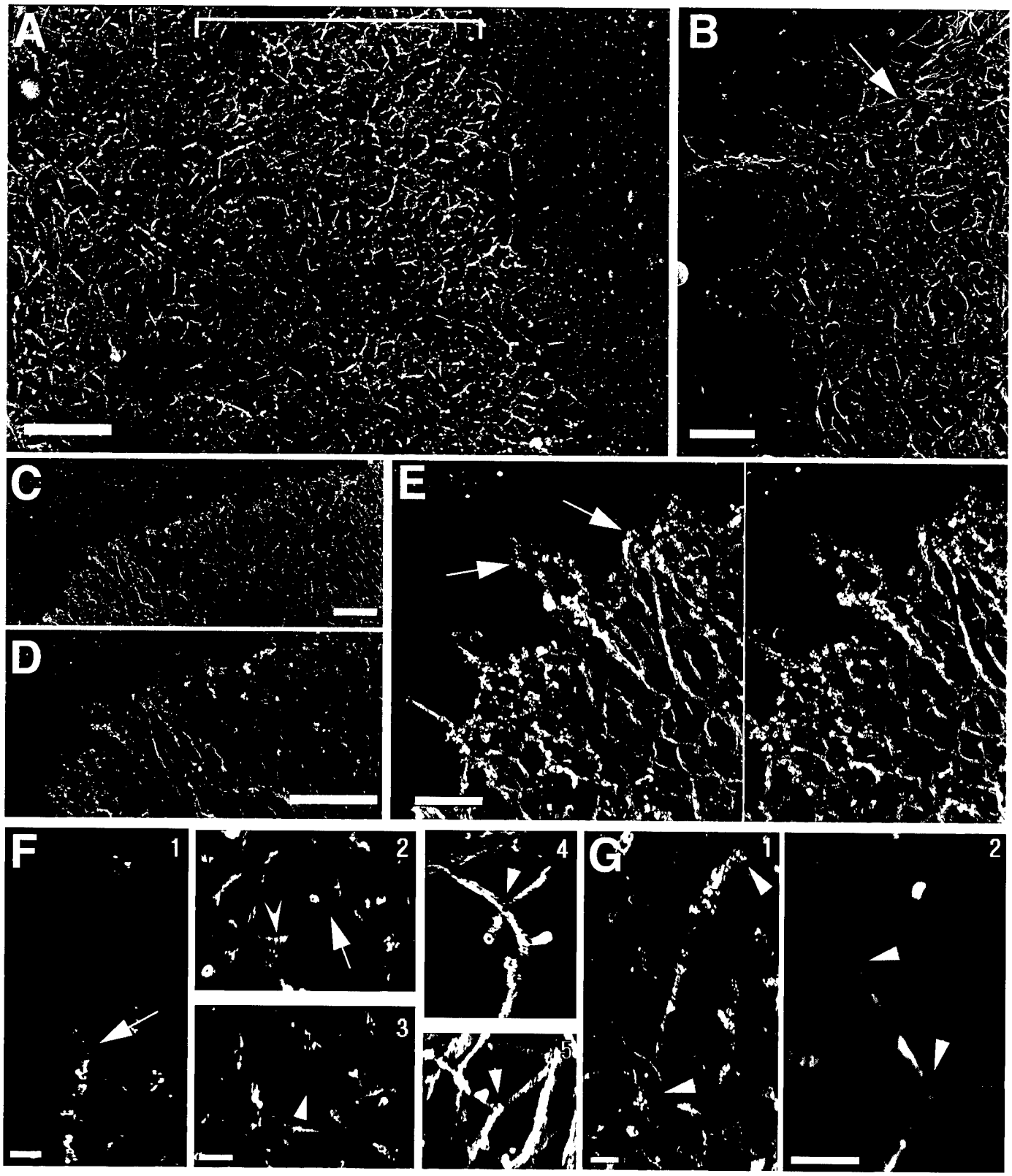

Figure 8

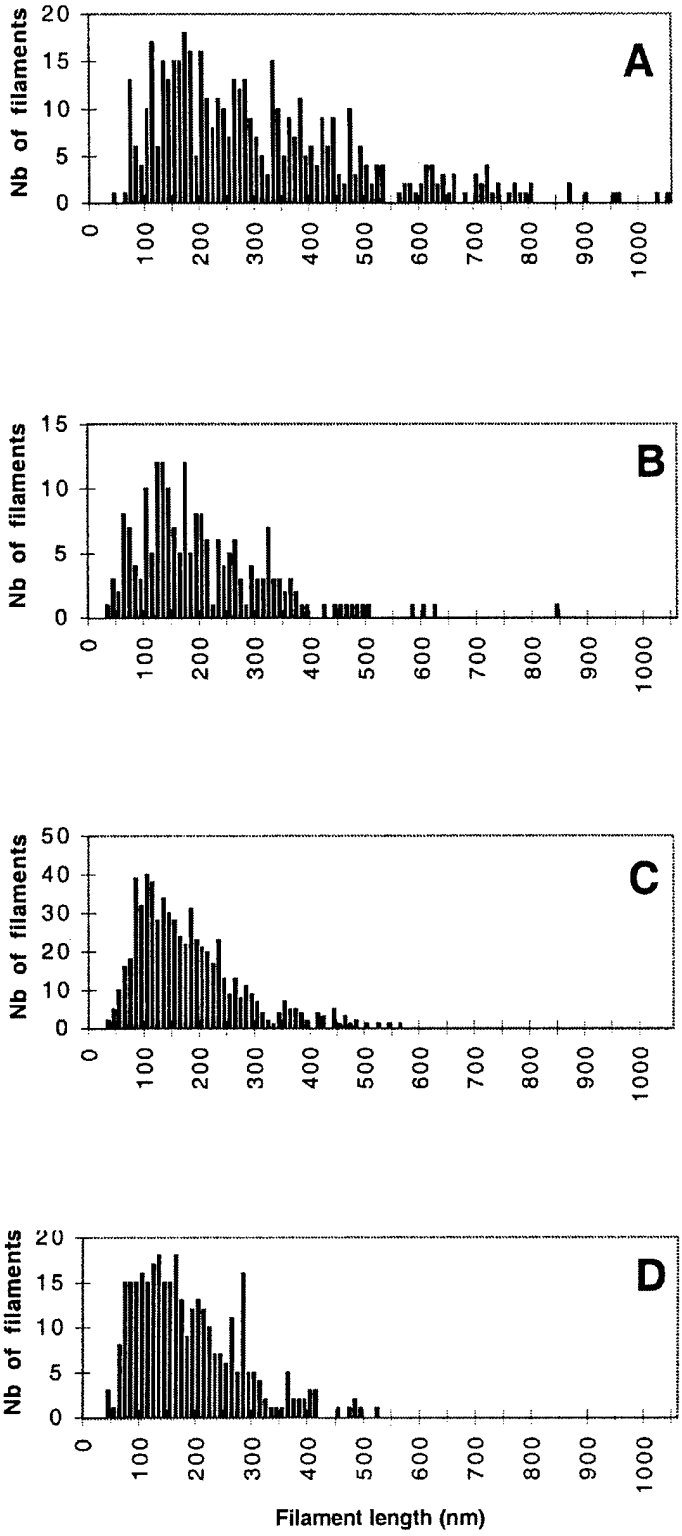
A
B
C
D
Nb of filaments
Filament length (nm)
0
100
200
300
400
500
600
700
800
900
1000

Figure 9

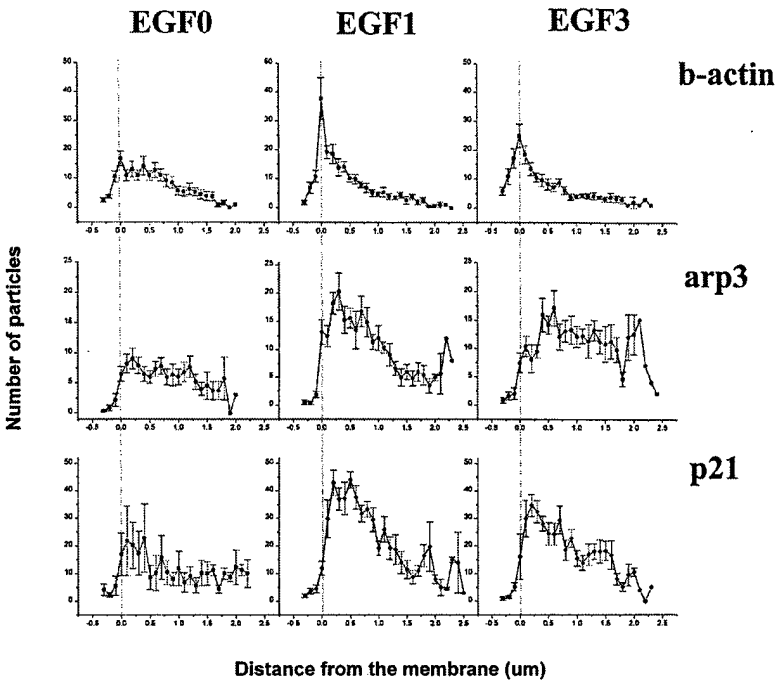

Figure 10

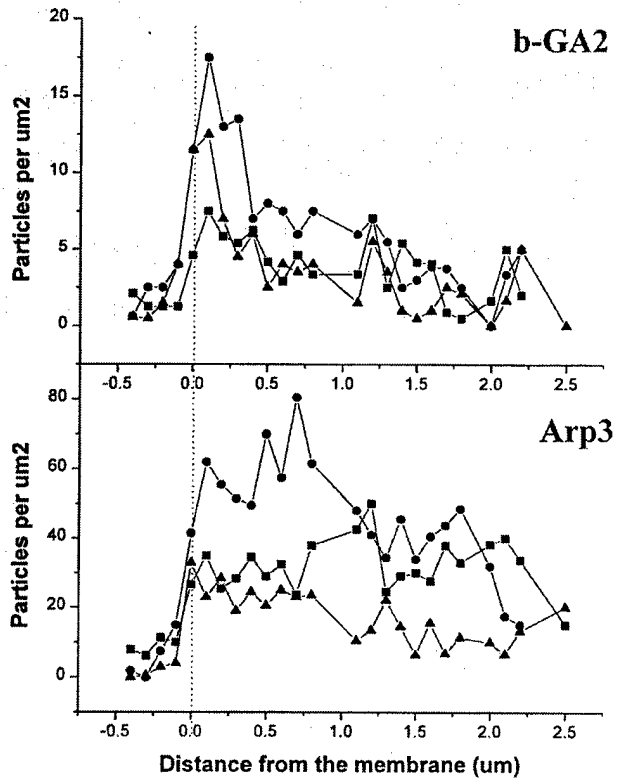

Figure 11

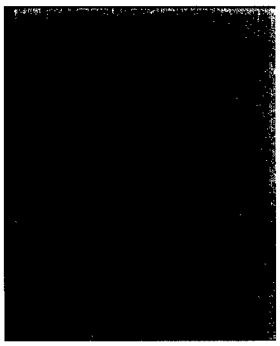

Figure 13

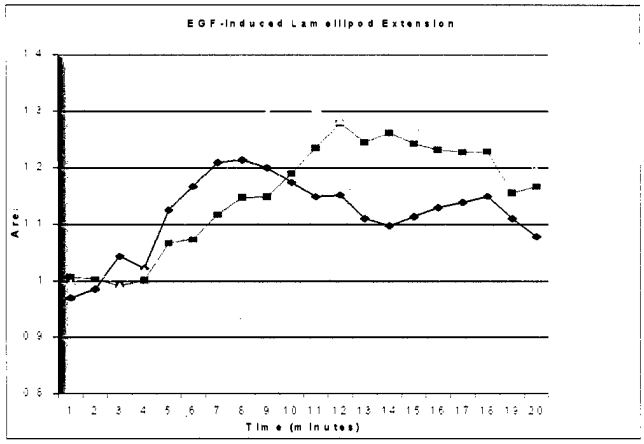

Figure 12

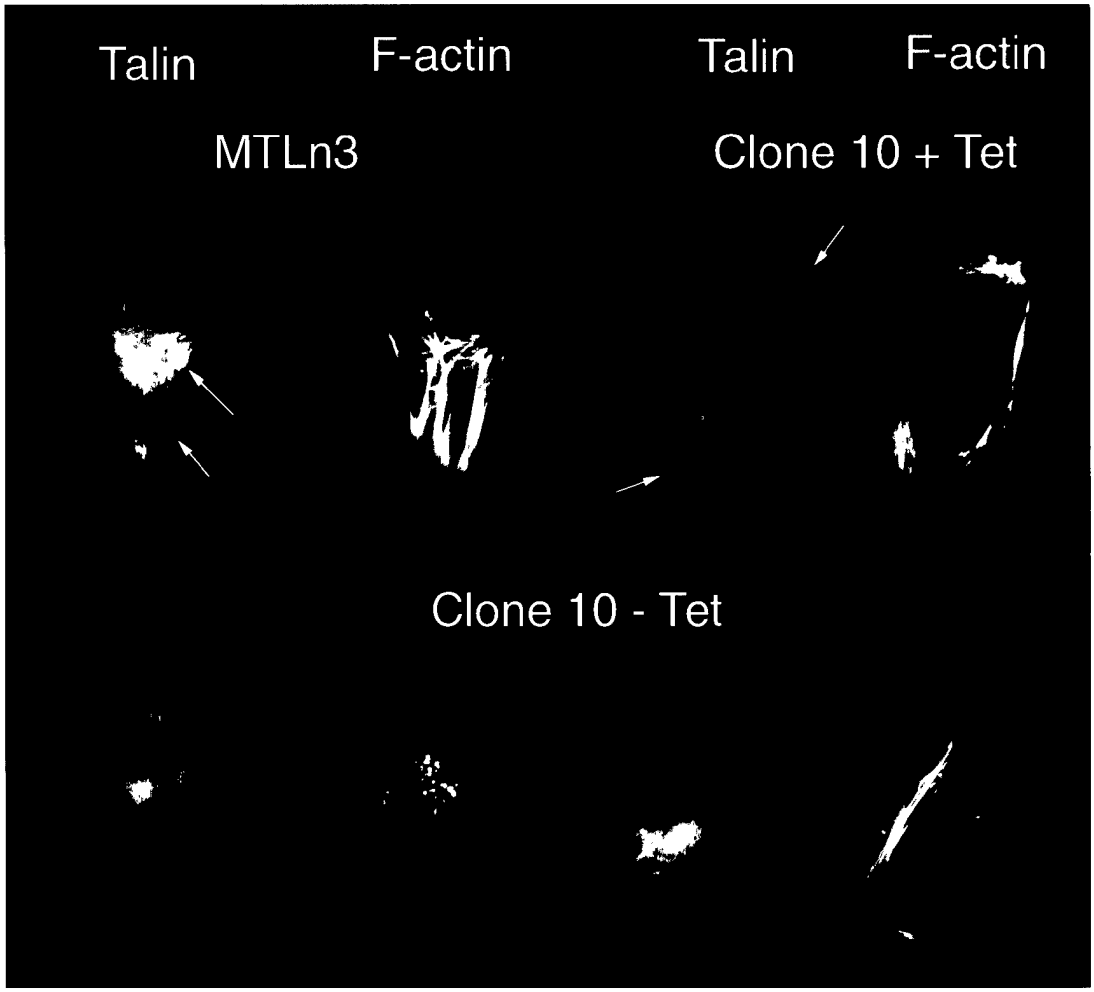

Figure 14

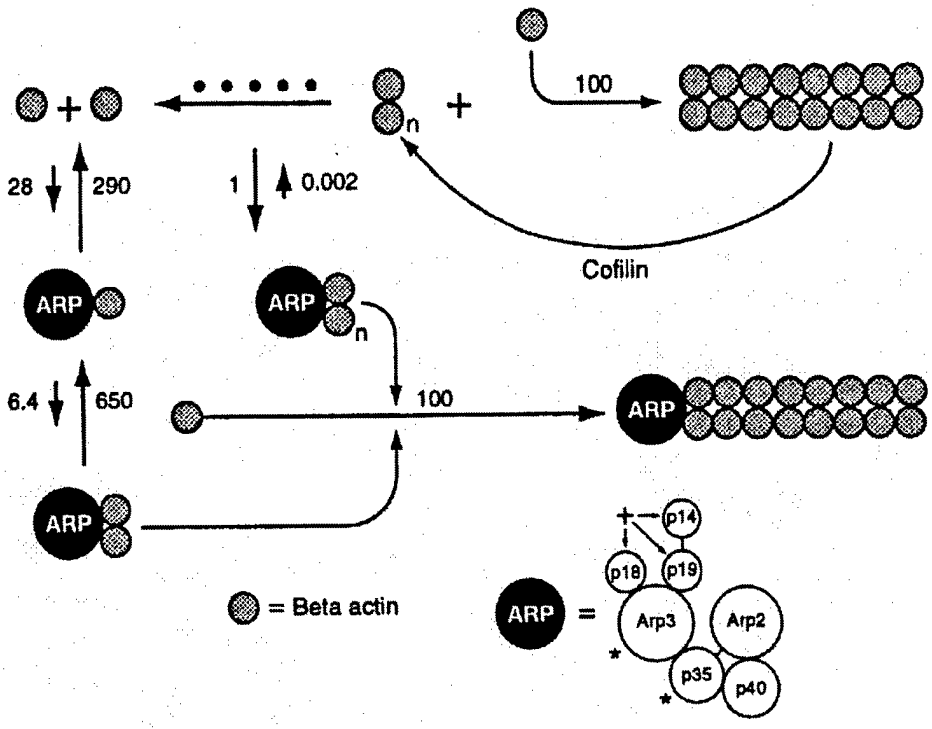
100
n
28
290
1
0.002
Cofilin
ARP
ARP
n
6.4
650
100
ARP
ARP
= Beta actin
ARP =
p14
p18
p19
Arp3
Arp2
p35
p40

Figure 15

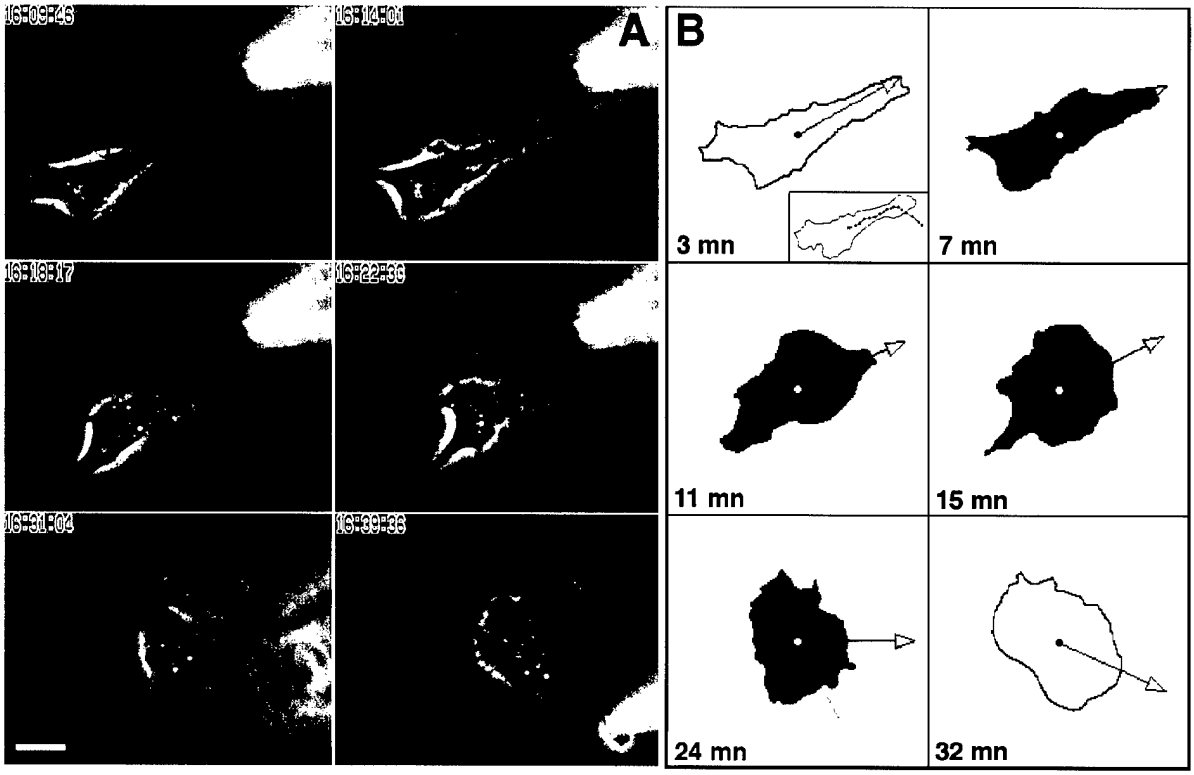

Figure 16

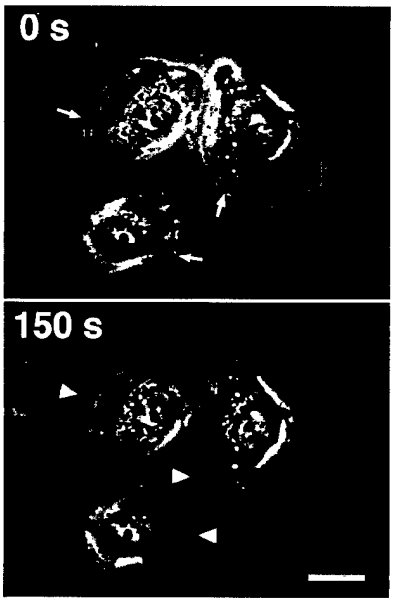

Figure 17

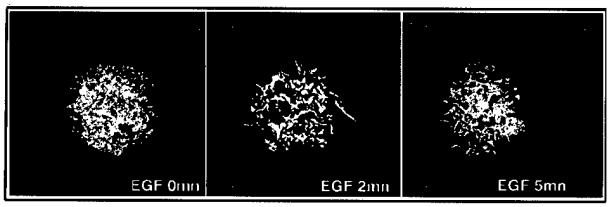

Figure 18

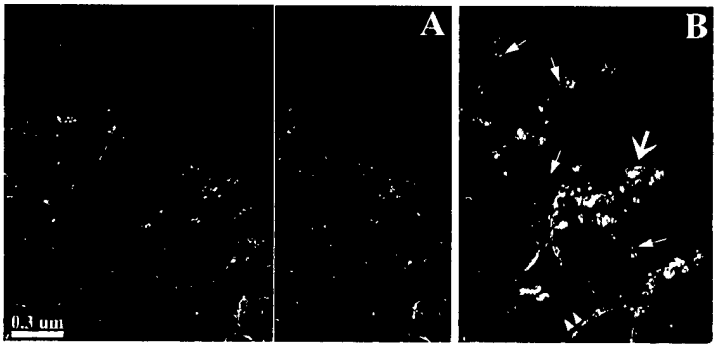

Figure 19

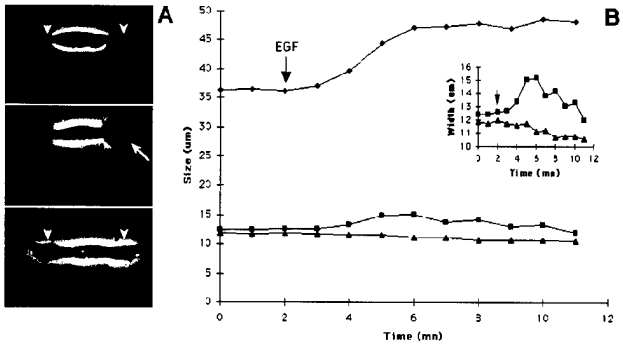

Figure 20

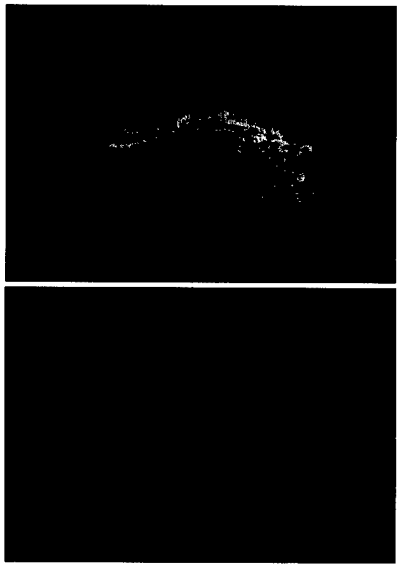

Figure 21

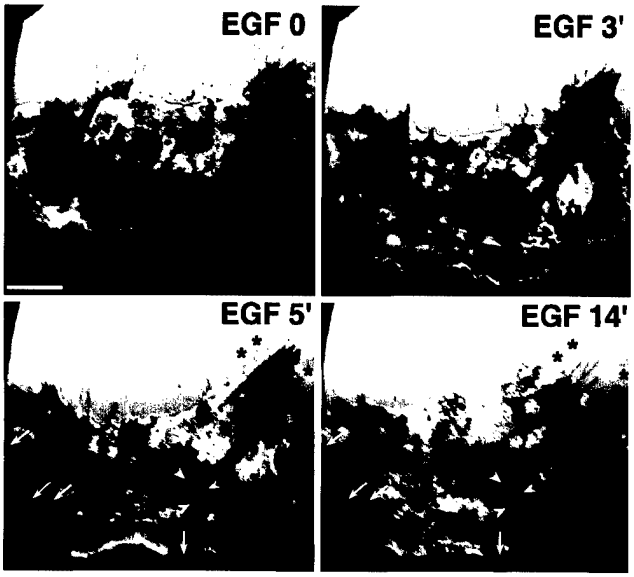

Figure 22

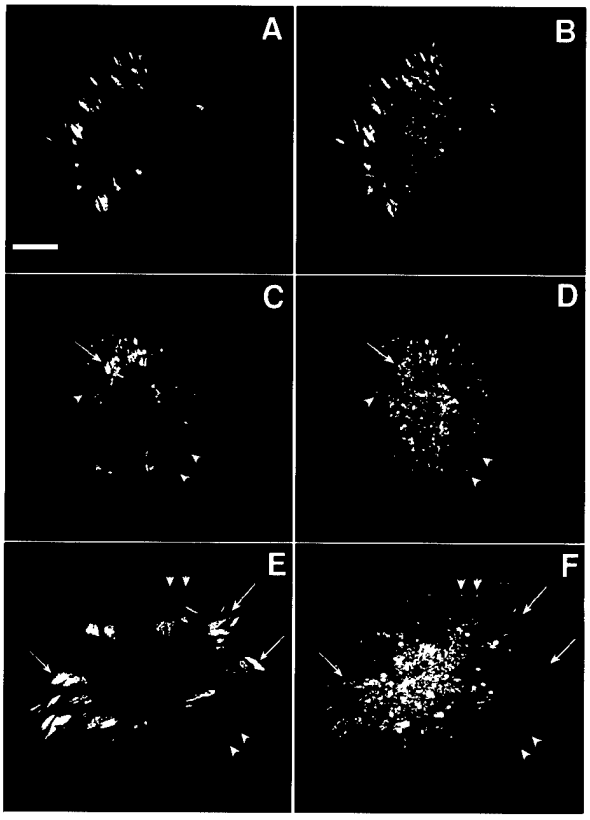

Figure 23